The Astrophysical Journal, 680:312–327, 2008 June 10

HYPERVELOCITY STARS: FROM THE GALACTIC CENTER TO THE HALO

Scott J. Kenyon
Smithsonian Astrophysical Observatory, 60 Garden Street, Cambridge, MA 02138; skenyon@cfa.harvard.edu

Benjamin C. Bromley
Department of Physics, University of Utah, 115 S 1400 E, Room 201, Salt Lake City, UT 84112; bromley@physics.utah.edu

and

Margaret J. Geller and Warren R. Brown
Smithsonian Astrophysical Observatory, 60 Garden Street, Cambridge, MA 02138; mgeller@cfa.harvard.edu, wbrown@cfa.harvard.edu
Received 2007 December 18; accepted 2008 February 21

ABSTRACT

Hypervelocity stars (HVSs) traverse the Galaxy from the central black hole to the outer halo. We show that the Galactic potential within 200 pc acts as a high-pass filter preventing low-velocity HVSs from reaching the halo. To trace the orbits of HVSs throughout the Galaxy, we construct two forms of the potential which reasonably represent the observations in the range 5–10^5 pc: a simple spherically symmetric model and a bulge-disk-halo model. We use the Hills mechanism (disruption of binaries by the tidal field of the central black hole) to inject HVSs into the Galaxy and to compute the observable spatial and velocity distributions of HVSs with masses in the range 0.6–4 $M_\odot$. These distributions reflect the mass function in the Galactic center, properties of binaries in the Galactic center, and aspects of stellar evolution and the injection mechanism. For 0.6–4 $M_\odot$ main-sequence stars, the fraction of unbound HVSs and the asymmetry of the velocity distribution for their bound counterparts increase with stellar mass. The density profiles for unbound HVSs decline with distance from the Galactic center approximately as r^{-2} (but are steeper for the most massive stars, which evolve off the main sequence during their travel time from the Galactic center); the density profiles for the bound ejecta decline with distance approximately as r^{-3}. In a survey with a limiting magnitude of $V \lesssim 23$, the detectability of HVSs (unbound or bound) increases with stellar mass.

Subject headings: binaries: general — Galaxy: center — Galaxy: halo — Galaxy: structure — stars: kinematics — stellar dynamics

1. INTRODUCTION

The components of the Milky Way sample the diverse forms of matter in the universe from the black hole at the dynamical center to the dark matter component of the halo. Hypervelocity stars (HVSs), a class of recently discovered objects, are a probe linking the central black hole and its history to the outer halo. HVSs probably originate from interactions with the black hole; they travel out into the halo and beyond, serving as tracers of the Galactic potential on scales from 5 to 10^5 pc.

To make testable predictions of the relationships between the observable properties of HVSs and aspects of the Galactic center and halo, we adopt the massive black hole (MBH)–binary star interaction first proposed by Hills (1988) as the injection mechanism for HVSs. We then explore the impact of the Galactic potential, the properties of binaries in the Galactic center, the mass function in the Galactic center, and stellar evolution on the observable spatial and velocity distributions of HVSs as a function of stellar mass.

1.1. *History and Challenges*

Hills (1988) showed that HVSs are inevitable when sufficiently tight binary stars are disrupted by the tidal field of the central MBH. Much later, Yu & Tremaine (2003) analyzed the production of HVSs and argued that the Hills production rates were excessive. They considered other mechanisms for the production of HVSs, including interactions of single stars with a binary central black hole.

Brown et al. (2005) reported the first discovery of a HVS. The star, SDSS J090745.0+024507, is leaving the Galaxy with a heliocentric radial velocity of 853 ± 12 km s^{-1} and has the largest velocity ever observed in the Milky Way halo. Subsequent photometry revealed that the object is a slowly pulsating B main-sequence star (Fuentes et al. 2006). Only interaction with a MBH can plausibly accelerate a 3 $M_\odot$ main-sequence B star to such an extreme velocity.

The Brown et al. (2005) discovery inspired further observations along with a wealth of theoretical models. Edelmann et al. (2005) discovered a hypervelocity main-sequence B star plausibly ejected from the LMC (see also Bonanos et al. 2008), and Hirsch et al. (2005) reported a helium-rich subluminous O star probably ejected from Sgr A*. These three discoveries were serendipitous.

Brown et al. (2006a) then carried out a targeted search for HVSs by using the SDSS to select faint B-type stars with lifetimes consistent with travel times from the Galactic center but that are not a normally expected stellar halo population. So far this extensive survey has yielded another seven HVSs (Brown et al. 2006a, 2006b, 2007a, 2007b). The velocity of each of these stars exceeds the escape velocity from the Milky Way.

The observational discoveries have inspired theorists to reconsider production mechanisms and ejection rates of HVSs. Ejection mechanisms include the original Hills binary encounter with a MBH (Hills 1988; Yu & Tremaine 2003; Bromley et al. 2006), encounters between single stars and binary black holes (Yu & Tremaine 2003; Sesana et al. 2006, 2007a, 2007b; Merritt 2006), encounters of single stars with an intermediate-mass black hole (IMBH) inspiraling toward a MBH (Hansen & Milosavljević 2003; Gualandris et al. 2005; Levin 2006; Baumgardt et al. 2006), and single-star encounters with a cluster of stellar mass

black holes (SMBHs) around a MBH (O'Leary & Loeb 2008). Recently, Lu et al. (2007) predicted hypervelocity ejection of tight binary stars in interaction with a central binary MBH. Discovery of a single tight binary HVS would be a strong indication of a central binary MBH.

Absent the discovery of a binary HVS, distinguishing among the ejection mechanisms requires predictions of the resulting spatial and velocity distribution of the HVSs along with computation of expected ejection rates (e.g., Sesana et al. 2006, 2007a). For example, the Hills (1988) mechanism may produce the largest velocities (Sesana et al. 2007a), and a binary black hole may produce an anisotropic distribution of ejecta (Sesana et al. 2006).

Dynamical and evolutionary considerations for stellar populations near the Galactic center also constrain HVS ejection mechanisms. For example, observations of the current population of B stars at the Galactic center favor the Hills (1988) mechanism over models involving an inspiraling IMBH or a cluster of SMBHs (Perets 2007).

Ejection rate estimates depend on an understanding of the way stars are scattered onto orbits intersecting the MBHs "loss cone" and on the specific ejection mechanism. Perets (2007) and Perets et al. (2007) argue that scattering by giant molecular clouds gives HVS production rates from binary disruption by a single MBH that are consistent with the observations.

In addition to the HVSs, all of the ejection mechanisms produce a bound population of ejecta (e.g., Bromley et al. 2006). Brown et al. (2007a, 2007b) demonstrate the very probable presence of a bound population of ejected B stars. These stars have velocities between 275 and 450 km s^{-1}. In this velocity range the Brown et al. surveys detect 18 outgoing stars and only 1 incoming star, consistent with the ~200–300 Myr lifetime of these main-sequence stars and a Galactic center origin (see also Svensson et al. 2008).

Because HVSs travel across the Galaxy, they are powerful tracers of the Galactic potential (Gnedin et al. 2005; Yu & Madau 2007). Yu & Madau (2007) emphasize that the population of bound and unbound ejecta constrains the anisotropy of the halo independent of the ejection mechanism.

The power of HVSs as probes of the Galactic center and as tracers of the Galactic potential provides strong motivation for acquisition of larger samples of these objects. Brown et al. focus on B stars because these objects are not an indigenous population in the halo, and they are observable to large distances where the contrast between the density of HVSs and any indigenous population is largest. Kollmeier & Gould (2007) suggest searches for possibly more numerous old-population, lower mass HVSs. Detection of lower mass HVSs could provide strong tests of models for their origin.

1.2. *From the Galactic Center to the Halo*

In the Hills (1988) mechanism, HVSs naturally sample both the stellar mass function and the properties of the binary population in the Galactic center. The ejecta then traverse the Galaxy and become observable in the halo. We show that the observable velocity and spatial distributions of HVSs are sensitive to the Galactic potential, particularly on scales of 5–200 pc from the Galactic center. These distributions also reflect stellar evolutionary timescales.

To include as complete a picture of the consequences of the Hills ejection mechanism as possible, we consider a broad range of issues in this paper. In § 2.1 we simulate the MBH-binary interaction following the procedures of Bromley et al. (2006). Motivated by Kollmeier & Gould (2007), we extend the simulations to cover lower mass stars and unequal-mass binaries. In § 2.2 we derive forms for the Galactic potential which are a good representation of the observations from 5 to 10^5 pc. Our results show that most of the deceleration of HVSs occurs within the central 200 pc of the Galaxy; thus, a proper fit to the observations in this region is a crucial step in understanding HVSs.

In §§ 2.3, 2.4, and 2.5, respectively, we describe our integration of HVS orbits through the Galaxy, the procedure we use to construct mock catalogs of HVSs, and the impact of azimuthal deflections on HVS orbits.

We continue with more detailed discussions of the observable properties of HVSs in a simple spherically symmetric potential (§ 3) and in a three-component Galaxy (§ 4). One of the most striking general results of this investigation is that a central potential which matches observations in the central 200 pc of the Galaxy acts as a high-pass filter preventing lower velocity HVSs from reaching the halo.

In §§ 3 and 4 we predict the spatial and velocity distributions of HVSs as a function of stellar mass, and we address the underlying physical explanations for the behavior of these distributions. In § 5 we connect the predictions with the observations by calculating relative space densities as a function of stellar mass (§ 5.1). This discussion emphasizes that the relative numbers of bound stars are sensitive to the mass function in the Galactic center and relative stellar lifetimes; relative numbers of unbound stars are nearly independent of stellar lifetimes.

In §§ 5.2 and 5.3 we analyze some sample HVS search approaches. We argue that searches become increasingly difficult with decreasing stellar mass (§ 5.2). We also demonstrate that short lifetimes make the discovery of post-main-sequence HVSs unlikely. We conclude in § 6.

2. THE SIMULATIONS

In Bromley et al. (2006) we developed initial methods for predicting the observable velocity distribution of HVSs in the Galactic halo. We derived ejection velocities appropriate for a single MBH disrupting binaries with 3–4 $M_\odot$ primary stars and a realistic range of initial binary semimajor axes, $a_{\rm bin}$. We then adopted a simple prescription for the Galactic mass distribution, integrated the orbits of stars ejected from the Galactic center, and computed a first approximation to the full observable phase-space distribution of ejected stars on radial orbits in the halo. This analysis showed that the predicted median speeds of ejected stars as a function of distance in the halo are consistent with current observations. We also predicted a population of ejected stars on bound radial orbits, then discovered by Brown et al. (2007a) as a 3.5 σ excess of B-type main-sequence stars with velocities of 275–400 km s^{-1}.

Here, we extend our analysis to consider a wider range of binary star masses and several Galactic potentials. Our goals are (1) to understand the relative frequencies of HVSs and bound ejected stars as a function of stellar mass and (2) to explore the sensitivity of observable HVS radial velocities on the Galactic potential from 5 to 10^5 pc.

As in Bromley et al. (2006), we simulate the ejection of stars from the Galactic center in three steps. Following Hills (1988, 1992), we integrate orbits of binary stars passing by Sgr A^* to quantify ejection probabilities and velocities. Then we use a Monte Carlo code based on semianalytical approximations for rapid generation of simulated catalogs of ejected stars in the Galactic center. Finally, we integrate the orbits of these stars in the Galactic potential to calculate how they populate the Galaxy's halo.

To generate observable samples, the simulation incorporates the stellar main-sequence lifetime from published stellar evolution calculations. We depart from Bromley et al. (2006) by

TABLE 1
Adopted Properties of Main-Sequence Binary Stars

Mass ($M_\odot$)	t_{ms} (Gyr)	R_{ms} ($R_\odot$)	$a_{min,q=1}$ (AU)	$a_{min,m_2=0.6}$ (AU)
0.6	13	0.6	0.015	0.015
1	10	1.3	0.032	0.029
1.5	2.9	2.5	0.061	0.051
2	1.2	3.3	0.081	0.063
3	0.35	4.7	0.115	0.084
4	0.16	5.5	0.134	0.100

Note.—These parameters are described in § 2.1.

considering primary and secondary stars with masses m_1 and m_2 in the range 0.6–4 $M_\odot$. In addition to considering orbits of stars in a simple spherical Galaxy, we also derive velocity distributions for stars ejected into a standard Galactic potential consisting of a bulge, disk, and extended halo.

2.1. *Massive Black Hole–Binary Star Interaction*

To obtain the spectrum of ejection speeds as a function of the properties of the disrupted binary star, we first simulate the MBH-binary interaction. As in Bromley et al. (2006), we use a sixth-order symplectic integrator (Yoshida 1990; Bromley & Kenyon 2006; Kenyon & Bromley 2006) to simulate the disruption of a binary system falling into a MBH with mass $M_\bullet = 3.5 \times 10^6\ M_\odot$ (e.g., Ghez et al. 2005). The binaries have a random orbital axis and phase; the semimajor axis is in the range $a_{bin} = (a_{min}, a_{max})$, where a_{min} depends on the binary mass and $a_{max} \approx 4$ AU. We assume that the center of mass of the binary is on a hyperbolic orbit with an initial approach speed of 250 km s^{-1} (Hills 1988) and that the binary has negligible orbital eccentricity.

Motivated by Kollmeier & Gould (2007), we extend our simulations to equal-mass binaries with lower mass primary stars and to unequal-mass binaries (Table 1). Table 1 includes the main-sequence lifetime t_{ms}, the stellar radius at the time of core hydrogen exhaustion R_{ms}, and the minimum a_{bin} for a binary with unit mass ratio $q \equiv m_1/m_2 = 1$ (Schaller et al. 1992; Schaerer et al. 1993). To minimize the probability of a collision during the encounter ($\lesssim$10%), we set $a_{min} = 2R_{ms,1}/r_L$ (see also Table 1 of Ginsburg & Loeb 2007), where $R_{ms,1}$ is the radius of the primary star and

$$r_L = \frac{0.49q^{2/3}}{0.6q^{2/3} + \ln(1 + q^{1/3})} \quad (1)$$

is the fractional radius of the inner Lagrangian surface for a binary system with a circular orbit (Eggleton 1983). This assumption allows us to sample a wide range of binary systems without worry that the interaction with the central black hole leads to tidal interaction between the binary components and possible coalescence (Ginsburg & Loeb 2007). Table 1 also lists a_{min} for unequal-mass binaries with 0.6 $M_\odot$ secondary stars.

Our calculations reproduce published results, and they are consistent with analytical estimates of HVS production (Hills 1988, 1992; Yu & Tremaine 2003; Gould & Quillen 2003). The median ejection velocity measured at infinity is

$$v_{ej} = 1760 \left(\frac{a_{bin}}{0.1\ \mathrm{AU}}\right)^{-1/2} \left(\frac{m_1 + m_2}{2\ M_\odot}\right)^{1/3} \left(\frac{M_\bullet}{3.5 \times 10^6\ M_\odot}\right)^{1/6} f_R\ \mathrm{km\ s^{-1}}, \quad (2)$$

where m_1 is the mass of the primary star and m_2 is the mass of the secondary star. The factor f_R is a normalization factor that depends on r_{close}, the distance of closest approach to the black hole,

$$f_R = 0.774 + \Big(0.0204 + \Big\{-6.23 \times 10^{-4} + \big[7.62 \times 10^{-6} + (-4.24 \times 10^{-8} + 8.62 \times 10^{-11} D)D\big]D\Big\}D\Big)D, \quad (3)$$

where

$$D = \left(\frac{r_{close}}{a_{bin}}\right)\left[\frac{2M_\bullet}{10^6(m_1 + m_2)}\right]^{-1/3}. \quad (4)$$

This factor also sets the probability for an ejection, P_{ej},

$$P_{ej} \approx 1 - D/175 \quad (5)$$

for $0 \le D \le 175$. For $D > 175$, $r_{close} \gg a_{bin}$; the binary does not get close enough to the black hole for an ejection, and $P_{ej} \equiv 0$.

For any binary system, the ejection probability and median ejection speed are set by the binary parameters a_{bin}, m_1, and m_2 and the distance of closest approach to the black hole r_{close}. We assume that we can ignore the chance of a merger event between binary companions and that ejections of the primary and secondary star are equally likely. Because they can only occur in rare cases where a_{bin} and r_{close} are both small (e.g., Ginsburg & Loeb 2006, 2007), mergers are unlikely to change our results by more than 10%.

Our simulations suggest that the binary mass ratio affects the ejection probability only when the mass ratio is extreme ($m_1/m_2 > 10$). There is then a consistent preference for ejection of the secondary (for additional details, see Bromley et al. 2006). When the binary contains unequal-mass stars, the median ejection speeds of the primary and secondary stars are

$$v_1 = v_{ej}\left(\frac{2m_2}{m_1 + m_2}\right)^{1/2} \quad \text{and} \quad v_2 = v_{ej}\left(\frac{2m_1}{m_1 + m_2}\right)^{1/2}, \quad (6)$$

respectively. In all cases, the distribution of ejection speeds is approximately Gaussian with a dispersion of 20% of the median speed.

2.2. *The Galactic Potential*

Once ejected stars leave the central black hole, they travel out through the Galaxy and decelerate. Historically, mass models for the Galaxy developed for other applications have been optimized to fit observations at distances $r \gtrsim 200$ pc from the Galactic center (e.g., Dehnen & Binney 1998; Klypin et al. 2002; Yu & Tremaine 2003; Widrow & Dubinski 2005). For ejected stars, however, the largest deceleration occurs in the central 200 pc (see Fig. 1). Thus, we need a Galaxy model that reproduces the Galactic potential within 200 pc of the Galactic center.

In their analysis of the proper motion of Arches, a cluster of young stars in the Galactic center, Stolte et al. (2008) also realized that standard Galactic potential models are inadequate to address dynamical phenomena in the Galactic center. They derive a three-component triaxial model for the central Galaxy which allows them to investigate the orbits of Arches stars in the central potential. However, their application does not depend on an accurate potential beyond the Galactic center; thus, their parameters do not match the potential at $r \gtrsim 0.5$–1 kpc.

Because HVSs traverse the Galaxy, we need a potential that fits observations from the Galactic center to the outer halo. Thus,

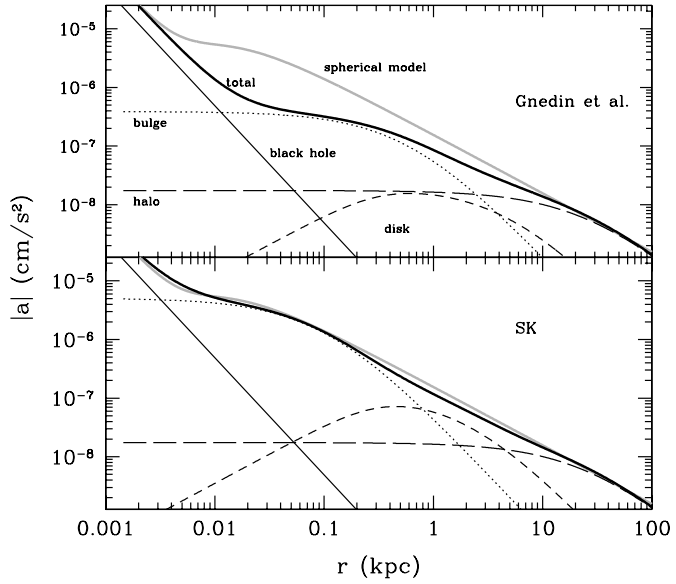

FIG. 1.—Acceleration in the Galactic potential. *Bottom*: Decomposition of our Galaxy potential into contributions from the central black hole (*thin solid black line*), bulge (*dotted line*), disk (*short-dashed line*), and halo (*long-dashed line*). The thick solid black line indicates the combined potential for comparison with the simple spherical potential (*thick gray line*). *Top*: Same as bottom panel but for the Gnedin et al. (2005) Galaxy potential.

we derive Galaxy models that fit both the observations at 5–200 pc (where HVSs decelerate considerably) and at 10–100 kpc (where we observe HVSs today).

2.2.1. *Parameterization of the Galactic Potential*

We consider two parameterizations of the Galaxy potential. First, we follow Bromley et al. (2006) and adopt a simple, spherically symmetric density profile,

$$\rho(r) = \frac{C}{1 + (r/r_c)^2}. \tag{7}$$

To yield a mass of $\sim 3 \times 10^7\ M_\odot$ within 10 pc of the Galactic center (as inferred from stellar kinematics; Eckart & Genzel 1997; Launhardt et al. 2002; Schödel et al. 2003; Ghez et al. 2005) and a circular rotation speed of 220 km s^{-1} in the solar neighborhood (Hogg et al. 2005), we adopt[1] $r_c = 8$ pc and $C = 1.396 \times 10^4\ M_\odot\ \mathrm{pc}^{-3}$. This density profile yields a mass of $\sim 1.2 \times 10^9\ M_\odot$ inside 120 pc, compared to an estimate of $(8 \pm 2) \times 10^8\ M_\odot$ in the nuclear stellar disk (Launhardt et al. 2002). The corresponding potential is

$$\Phi_G(r) = -2\pi G C r_c^2 \left[2(r_c/r)\arctan(r/r_c) + \ln\left(1 + r^2/r_c^2\right)\right], \tag{8}$$

where G is the gravitational constant. If we add the potential of the central black hole, the total potential is

$$\Phi(r) = \Phi_G(r) - GM_\bullet/r. \tag{9}$$

To examine the impact of Φ on our results, we also consider a three-component, spherically symmetric potential that includes contributions from the bulge (Φ_b), disk (Φ_d), and halo (Φ_h) (e.g., Gnedin et al. 2005; Widrow & Dubinski 2005). Specifically, we adopt

$$\Phi_G = \Phi_b + \Phi_d + \Phi_h, \tag{10}$$

where

$$\begin{aligned} \Phi_b(r) &= -GM_b/(r + a_b), \\ \Phi_d(R,z) &= -GM_d/\sqrt{R^2 + \left[a_d + \left(z^2 + b_d^2\right)^{1/2}\right]^2}, \\ \Phi_h(r) &= -GM_h \ln(1 + r/r_s)/r \end{aligned} \tag{11}$$

(e.g., Hernquist 1990; Miyamoto & Nagai 1975; Navarro et al. 1997). Here, r is the radial coordinate in a spherical coordinate system and (R, z) are cylindrical coordinates.

To choose appropriate parameters for this potential, we consider multicomponent mass models for the Galaxy. Most derivations adopt analytic functions for the mass density, $\rho(R, z)$, and then derive fitting parameters from least-squares fits to a set of dynamical observables (e.g., Dehnen & Binney 1998; Klypin et al. 2002; Battaglia et al. 2005; Dehnen et al. 2006). Widrow & Dubinski (2005) expand on this technique with an iterative approach that solves for a stable, self-consistent bulge-disk-halo model which fits the standard observables (see also Widrow et al. 2008). Although both of these approaches fit the data well for Galactic center distances ranging from ~200 pc to ~100–200 kpc, they are not optimized for the Galactic center region at ~5–200 pc (see also Stolte et al. 2008).

Here, we derive a potential model that provides a reasonable match to observations throughout the range 5–10^5 pc. Table 2 lists our results. We follow Gnedin et al. (2005) and adopt disk[2] and halo parameters from Klypin et al. (2002). For the bulge, we derive parameters that fit the velocity dispersion data at 5–200 pc (Tremaine et al. 2002), the mass within 10 pc inferred from stellar kinematics (Eckart & Genzel 1997; Launhardt et al. 2002; Genzel et al. 2003; Schödel et al. 2003; Ghez et al. 2005), and the mass of the nuclear stellar disk inside 120 pc [$(8 \pm 2) \times 10^8\ M_\odot$; Launhardt et al. 2002]. Using a Newton-Raphson method that overweights measurements in the central 100 pc, we derive $M_b = 3.55 \times 10^9\ M_\odot$ and $r_b = 106$ pc.

This model for the bulge underestimates the stellar mass within a few parsecs of the Galactic center (Genzel et al. 2003). Because mass in the central 10–100 pc has the largest impact on HVS trajectories, this underestimate has little impact on our results.

Table 2 compares the parameters for our Galaxy model with other models used for calculations of HVS trajectories. Yu &

TABLE 2
PARAMETERS FOR THREE-COMPONENT GALAXY POTENTIALS

Paper	M_b ($10^9\ M_\odot$)	r_b (kpc)	M_h ($10^{12}\ M_\odot$)	r_h (kpc)	M_d ($10^{10}\ M_\odot$)	a_d (kpc)	b_d (kpc)
DB98	2.50	0.05	0.8	21.8	5.0	2.4	0.18
GG05	10.00	0.60	1.0	20.0	4.0	5.0	0.30
YM07	10.00	0.50	1.4	25.9	4.0	5.0	0.30
This paper	3.76	0.10	1.0	20.0	4.0	2.0	0.30

NOTES.—These parameters are described in § 2.2 and eq. (11). The cited models are DB98, Dehnen & Binney (1998); GG05, Gnedin et al. (2005); and YM07, Yu & Madau (2007).

[1] Although Bromley et al. (2006) used the value for C quoted here in their numerical simulations, they quoted $C = 1.27 \times 10^4$ in the text. Here, we quote the correct value for C.

[2] To maintain a circular velocity of 220 km s^{-1} at 8 kpc, we reduce the disk scale length from 5 to 4 kpc.

TABLE 3
Mass-Radius Relation for Milky Way

Model	M_{10} ($10^7\ M_\odot$)	M_{120} ($10^9\ M$)	M_{210} ($10^9\ M_\odot$)	M_{8000} ($10^{10}\ M_\odot$)	$M_{100,000}$ ($10^{12}\ M_\odot$)
Target.....	3.0	0.8	2.7	9.0	0.7
BKG06.....	2.9	1.2	2.2	9.0	1.1
This paper.....	3.0	1.1	1.8	8.2	1.0
DB98.....	2.1	0.4	0.9	9.0	0.6
WD05.....	7.0	1.3	2.7	9.0	0.7
GG05.....	0.3	0.3	0.7	8.2	1.0
YM07.....	0.3	0.3	0.7	7.8	1.2
SGM07.....	2.3	1.1	2.4	...	...

Notes.—These parameters are described in § 2.2. References are as follows: DB98, Dehnen & Binney (1998); GG05, Gnedin et al. (2005); YM07, Yu & Madau (2007); WD05; Widrow & Dubinski (2005); BKG06, Bromley et al. (2006); and SGM07, Stolte et al. (2008).

Madau (2007) adopt the Klypin et al. (2002) parameters for the bulge and disk and the Diemand et al. (2007) halo model. For the Dehnen & Binney (1998) multicomponent triaxial potential, we derive the best-fitting spherical, three-component model for the radial component of their potential. Our mass and scale length for the bulge agree well with the Dehnen & Binney (1998) model.

Table 3 compares the mass-radius relations for several Milky Way models with observations. For the observed masses—listed as "Target" in the table—enclosed within 10 pc (M_{10}) and 120 pc (M_{120}), we adopt the kinematic mass from Ghez et al. (2005) and the mass of the nuclear stellar disk from Launhardt et al. (2002). For the mass enclosed within $r = 210$ pc (M_{210}), we use the measured velocity dispersion at 210 pc (136 km s^{-1}; Tremaine et al. 2002; Widrow & Dubinski 2005) and make the conversion $M_{210} = 3rv^2/G$. At larger radii, we adopt the circular rotation speed of 220 km s^{-1} at $r = 8$ kpc (for M_{8000}; Hogg et al. 2005) and the Klypin et al. (2002) Milky Way mass at 100 kpc (for $M_{100,000}$). Aside from a low value at 210 pc, our mass model provides a good match to the target values. The Stolte et al. (2008) results provide a better match at 210 pc but underestimate the mass at 10 pc. Most other mass models (e.g., Dehnen & Binney 1998; Gnedin et al. 2005; Yu & Madau 2007) underestimate the mass substantially for all $r \lesssim 210$ pc. The Widrow & Dubinski (2005) models match the target data outside ~120 pc, but they overestimate the mass inside 100 pc (see their Fig. 6).

2.2.2. *Impact of the Central Potential on HVS Trajectories*

The radial variation of the acceleration, $a = \Phi/r$, demonstrates the importance of the central 200 pc of the Galactic potential in the ejection of HVSs (Fig. 1). For $r \lesssim 4$ pc, the central black hole dominates the deceleration of ejected stars (Tremaine et al. 2002; Widrow & Dubinski 2005). At larger radii, the acceleration has a clear plateau with a radial width comparable to the scale length r_b and then falls rapidly. For $r \gtrsim 5r_b$–$10r_b$, the disk and halo provide most of the deceleration. Although the disk adds to the halo component at $r \sim 1$–20 kpc, its contribution is always relatively small.

To illustrate how the acceleration varies among different potentials, Figure 1 compares $|a|$ for our simple spherical potential with the three-component model adopted here and a three-component model developed to analyze HVS trajectories in a triaxial Milky Way halo (Gnedin et al. 2005). Most other Galaxy potentials have acceleration profiles similar to the Gnedin et al. (2005) potential (e.g., Dehnen & Binney 1998; Klypin et al. 2002; Battaglia et al. 2005; Dehnen et al. 2006; Yu & Madau 2007). Because the Widrow & Dubinski (2005) potential overestimates the mass in the Galactic center, this model overestimates $|a|$ in the Galactic center.

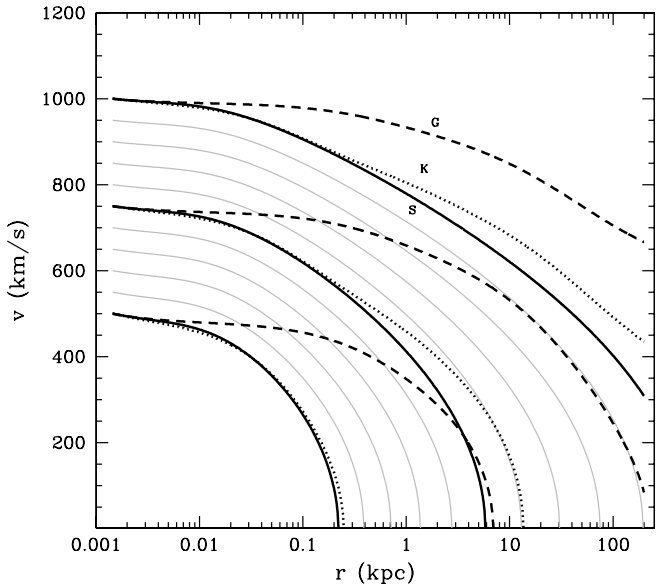

Fig. 2.—Radial velocity profiles of ejected stars in different Galaxy potentials. The labels indicate profiles in the Gnedin et al. (2005) potential (G), our three-component potential (K), and the simple spherical potential (S). The differences in the three sets of profiles starting at $v_0 = 500$, 750, and 1000 km s^{-1} illustrate the impact of the central potential in setting the observable properties of HVSs in the Galactic halo.

Figure 1 (*top*) compares $|a|$ for the Gnedin et al. (2005) potential with our simple spherical model. The larger r_b for the Gnedin et al. (2005) potential yields a plateau with smaller acceleration ($|a| \sim 5 \times 10^{-7}$ cm s^{-2}) at $r \sim 20$–200 pc. At $r \gtrsim 1$–100 kpc, the acceleration from the disk and halo match the simple potential.

Figure 1 (*bottom*) compares $|a|$ from our simple spherical model to $|a|$ for our adopted three-component Galaxy. The relatively small scale length of our bulge yields a good match to the plateau ($|a| \sim 6 \times 10^{-6}$ cm s^{-2}) of the spherical model at small radii, $r \sim 5$–30 pc. The disk + halo potential matches the spherical model well at large distances, $r \gtrsim 1$–2 kpc.

The acceleration profile of the inner Galaxy has a clear impact on the ejection of HVSs into the outer Galaxy (Fig. 2). The solid lines in Figure 2 show $v(r)$, the variation of velocity with galactocentric distance for the simple spherical potential as a function of v_0, the initial ejection velocity at 1.45 pc. The figure also shows several results for our three-component Galaxy (*dotted curves*) and for the Gnedin et al. (2005) potential (*dashed curves*). For the simple spherical potential, ejected stars with $v_0 \lesssim 625$ km s^{-1} fail even to reach $r \sim 1$ kpc. Stars with 625 km s^{-1} $\lesssim v_0 \lesssim$ 800 km s^{-1} reach $r \sim 1$–10 kpc; stars with $v_0 \gtrsim 800$ km s^{-1} reach $r \gtrsim 10$ kpc. We derive similar results for our adopted three-component Galaxy. In the Gnedin et al. (2005) potential, stars with relatively small ejection velocities, 525 km s^{-1} $\lesssim v_0 \lesssim$ 750 km s^{-1}, can reach large halo distances, $r \sim 10$–100 kpc. Thus, the larger deceleration produced by a more realistic potential for the Galactic center leads to smaller $v(r)$ and less penetration of ejected stars into the halo.

From these results, we expect clear differences between the observable velocity histograms of stars ejected into the Gnedin et al. (2005) potential and the histograms of stars ejected into our three-component Galaxy model. We discuss this issue in more detail in §§ 3 and 4.

2.3. *Integration of Orbits through the Galaxy*

To generate populations of stars ejected from the Galactic center, we perform Monte Carlo simulations of $\sim 10^6$ stars on radial orbits starting a small distance away from the black hole Sgr A*. Following Bromley et al. (2006) we assume $a_{\rm bin}$ is distributed with equal likelihood per logarithmic interval (see also Abt 1983; Duquennoy & Mayor 1991; Heacox 1998) between $a_{\rm min}$ (Table 1) and $a_{\rm max} \approx 4$ AU. Consistent with the expectation of strong gravitational focusing of the orbit of the center of mass of the binary by Sgr A*, we choose the distance of closest approach, $r_{\rm close}$, from a distribution that varies as $r_{\rm close}$. For an adopted pair of stellar masses m_1 and m_2, the random $a_{\rm bin}$ and $r_{\rm close}$ yield the ejection probability $P_{\rm ej}$. If $P_{\rm ej}$ exceeds a random deviate, we choose an ejection velocity v_0 from a Gaussian distribution with average velocity $v_{\rm ej}$ and dispersion $0.2 v_{\rm ej}$.

To follow the trajectories of these ejected stars through the Galaxy, we use a simple leapfrog integrator (Bromley et al. 2006). We start each star on a radial trajectory with velocity v_0 at a distance of 1.45 pc from Sgr A*. For our adopted potential, the mass in stars within this radius from Sgr A* is roughly 5% of the black hole's mass (Table 3). Thus, our results are fairly independent of the starting position. Once the initial trajectory is set, we use the leapfrog integrator to derive the time-dependent velocity of the star through a Galaxy with potential Φ (eqs. [8] or [10]).

Simulations of HVSs with several potentials provide a better understanding of the physical processes involved in ejecting stars from the Galactic center into the Galactic halo. Calculations with the simple spherical potential (eq. [8]) allow us to isolate the impact of stellar evolution from the deceleration of ejected stars traveling through the Galaxy (§ 3). Simulations with the three-component Galaxy (eq. [10]) yield clear estimates for the sensitivity of observable quantities on the mass in the Galactic center and the triaxiality of the potential (§ 4).

2.4. *Predicting Observable Quantities*

To generate mock catalogs of HVSs, we assume that the central black hole ejects stars at a constant rate on timescales comparable to the typical orbital timescales of the bound population, $t_{\rm orb} \sim 1$ Gyr. We eject each star at a time $t_{\rm ej}$, randomly chosen between zero and the main-sequence lifetime of the primary star $t_{\rm ms,1}$, and observe each star at a time $t_{\rm obs}$, randomly chosen between zero and the main-sequence lifetime for the ejected star ($t_{\rm ms,ej}$). The first constraint ($t_{\rm ej} < t_{\rm ms,1}$) guarantees that the binary interacts with the central black hole before post-main-sequence evolution disrupts the binary. The second constraint ($t_{\rm obs} < t_{\rm ms,ej}$) guarantees that earthbound observers detect the ejected star before it evolves off the main sequence. If $t_{\rm ej} < t_{\rm obs}$, we assign an ejection speed v_0 to the ejected star and integrate its orbit through the Galaxy for a travel time $t_t = t_{\rm obs} - t_{\rm ej}$. For each ejected star with index i observed at time $t_{{\rm obs},i}$, the mock catalog includes the derived distance r_i, the initial ejection velocity v_{0i}, the radial velocity at time $t_{\rm obs} v_i$, and the orbital elements for bound stars.

Although this procedure for generating catalogs of HVSs differs from the method described in Bromley et al. (2006), it yields similar results. Motivated by the high star formation rate in young clusters near the Galactic center (e.g., Figer et al. 1999, 2002; Lang et al. 2005), we previously adopted a short timescale between formation and ejection, i.e., $t_{\rm ej} \ll t_{\rm ms,1}$ (Bromley et al. 2006). Because binary stars outside nearby star-forming regions can also encounter the black hole (e.g., Perets et al. 2007), here we adopt a less restrictive constraint on the ejection timescale ($t_{\rm ej} < t_{\rm ms,1}$). Direct comparisons of new catalogs with the Bromley et al. (2006) catalogs show negligible differences in the predicted median speeds as a function of distance from the Galactic center or in the velocity histograms of halo stars (see below). Thus, our simulations are relatively insensitive to assumptions concerning the ejection time from the Galactic center.[3]

2.5. *Azimuthal Deflection of HVS Trajectories*

With main-sequence lifetimes longer than a typical orbital timescale $t_{\rm orb} \sim 1$ Gyr, bound stars with masses smaller than $1.5\ M_\odot$ can make several passes through the Galactic center and, perhaps, interact with the central black hole or other stars near the Galactic center before returning to the halo. For the spherically symmetric potential of equation (7), we estimate that bound stars on trajectories that pass within 10 pc of Sgr A* have less than a 0.01% chance of passing within 10 AU of another star in the Galactic center. The probability of encountering a star outside of the 10 pc region is even smaller. With speeds $\sim$800–1000 km s^{-1} near the Galactic center, a bound ejected star must pass within 0.1 AU of another star to suffer a significant deflection of its orbit. Thus, bound ejected stars do not change their orbits in a spherically symmetric Galaxy (see also Yu & Madau 2007).

For the three-component Galactic potential, significant deflections of HVS trajectories occur only if the potential is not spherical. Although a triaxial halo potential can produce significant proper motions in a sample of HVSs (Gnedin et al. 2005), these produce little change in the radial component of the velocity in the halo. After several passages through the Galactic center, however, Yu & Madau (2007) note that a triaxial halo may redistribute a bound star's kinetic energy between the radial and angular velocity. For reasonable triaxial halo potentials, the observed radial velocities of ejected bound stars change by $\sim$10% (Yu & Madau 2007).

A triaxial bulge potential can have a more dramatic impact on the observed velocities of ejected and bound HVSs. Current data suggest the mass distribution near the Galactic center is not spherical (see Dehnen & Binney 1998; Klypin et al. 2002; Dehnen et al. 2006; Stolte et al. 2008 and references therein). Because it is easier to eject stars along the minor axis of a triaxial Galactic center potential (e.g., Figs. 1–3), we expect potentially large differences in the observable velocities of HVSs as a function of Galactic latitude. To estimate the magnitude of this effect, we derive predicted velocity distributions for ejected and bound stars in two different three-component Galaxy potentials below (§ 4).

3. OBSERVABLE EJECTED STARS IN A SIMPLE SPHERICALLY SYMMETRIC POTENTIAL

To isolate how the important physical effects of the ejection process relate to the observable properties of ejected stars, we begin with a discussion of the evolution of ejected stars in a simple, spherically symmetric Galaxy (eq. [7]). We describe the evolution in the three-component Galactic potential in § 4. We further restrict our analysis of observable properties to stars with $r \geq 10$ kpc, where current surveys can distinguish ejected stars from the indigenous halo population and where the observed radial velocity is nearly indistinguishable from the true radial velocity of ejected stars (e.g., Brown et al. 2006a, 2006b, 2007a, 2007b).

[3] We assume a constant Galactic potential. Because the Galaxy probably gains mass with time (e.g., Bullock & Johnston 2005), our estimates for the bound population of older, less massive stars are more uncertain than estimates for more massive stars.

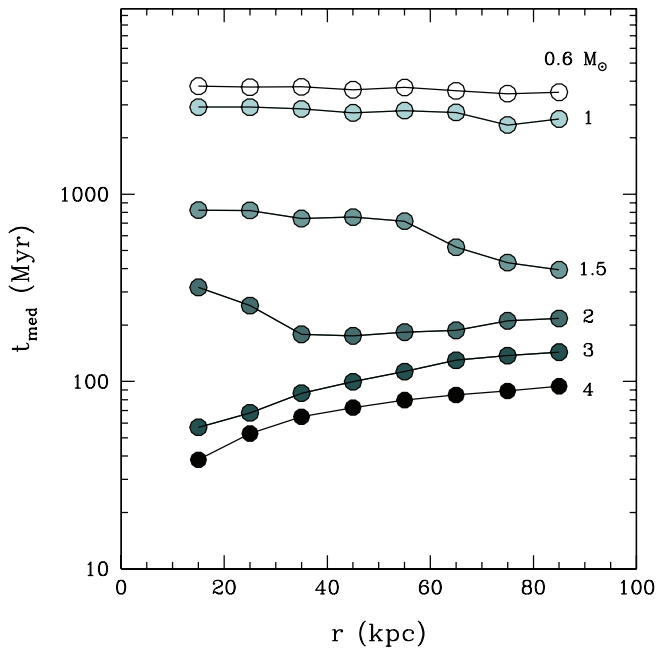

FIG. 3.—Median age of ejected stars on their first pass through the halo as a function of galactocentric distance. The labels indicate the masses of the ejected stars.

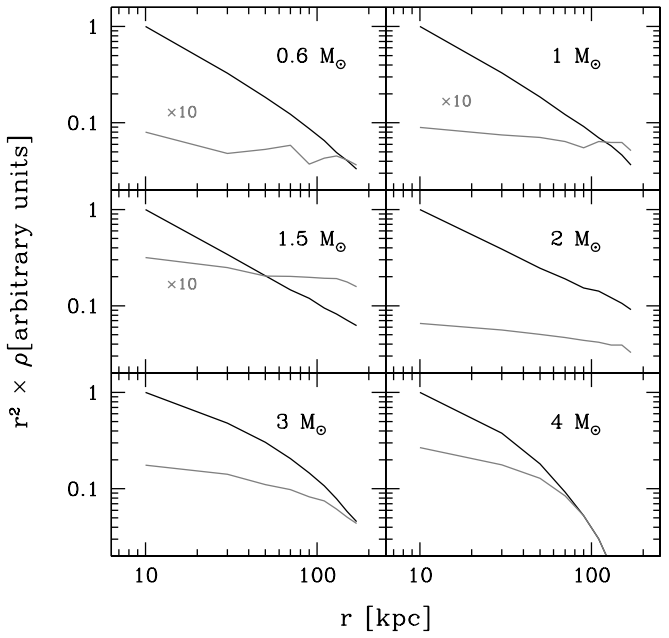

FIG. 4.—Relative density profiles of stars ejected from equal-mass binaries as a function of galactocentric distance. In each panel, the labels for all ejected stars (*black lines*) and for unbound stars (*gray lines*) indicate the mass of the ejected stars.

We divide these successful ejected stars into bound stars that orbit the Galactic center and unbound stars that leave the Galaxy. Because our forms for the Galactic potential do not yield true escape velocities, we define unbound stars as ejected stars that reach $r \gtrsim 200$ kpc with $v \gtrsim +200$ km s^{-1} (see Fig. 2). These stars have $v \gtrsim +450$ km s^{-1} at $r = 50$ kpc and $v \gtrsim +300$ km s^{-1} at $r = 100$ kpc.

With typical orbital periods of 1 Gyr, bound stars falling back into the Galactic center must have long lifetimes. Thus, bound stars are either low-mass stars or massive stars on their first pass out through the Galactic halo. For unbound stars, the typical travel times to $r \sim 40$–80 kpc are $\sim$100 Myr (Brown et al. 2007b). Thus, some 3–4 $M_\odot$ unbound stars with lifetimes of 150–350 Myr evolve off the main sequence while traveling through the halo. This evolution removes potential HVSs from the catalogs, reducing the relative frequency of massive stars at $r \gtrsim 50$–100 kpc (see below). Stellar evolution removes very few low-mass stars from the catalogs; thus, the observable properties of unbound 0.6–2 $M_\odot$ stars depend solely on the binary orbital parameters and the Galactic potential.

Figure 3 shows the median ages for stars ejected from equal-mass binaries on their first pass outward through the halo. Stars with radial speeds exceeding the escape velocity dominate the population of massive stars at all distances from the Galactic center. Thus, the observed median ages of 3–4 $M_\odot$ stars increase monotonically with r. Bound stars dominate the population of low-mass stars at all galactocentric distances. Thus, the median ages of 0.6–1 $M_\odot$ stars are roughly constant with r. For intermediate-mass stars, the median ages represent a mix of mostly bound stars at small r and mostly unbound stars at large r. The distribution of median ages for 2 $M_\odot$ stars is dominated by bound stars for $r \lesssim r_u \approx 20$ kpc and by unbound stars for $r \gtrsim r_u$, where r_u is the galactocentric distance for which the fraction of unbound stars exceeds 10%–15%. For 1.5 $M_\odot$ stars, the bound population dominates for $r \lesssim r_u \approx 70$–$80$ kpc. Thus, the median ages for 1.5–2 $M_\odot$ stars fall for $r \lesssim r_u$ and rise or remain constant for $r \gtrsim r_u$.

At large galactocentric distances, the radial distribution of ejected stars depends on the stellar mass and the shape of the Galactic potential (Fig. 4). Unbound stars (*gray lines*) are ejected at the largest possible velocities. They are the stars least affected by the Galactic potential and thus have shallow density profiles. For long-lived, low-mass stars, the density profile of unbound stars is slightly steeper than the $\rho \propto r^{-2}$ expected for a pointlike potential. Bound stars are ejected at smaller velocities and reach smaller galactocentric distances than unbound stars. Thus, bound stars

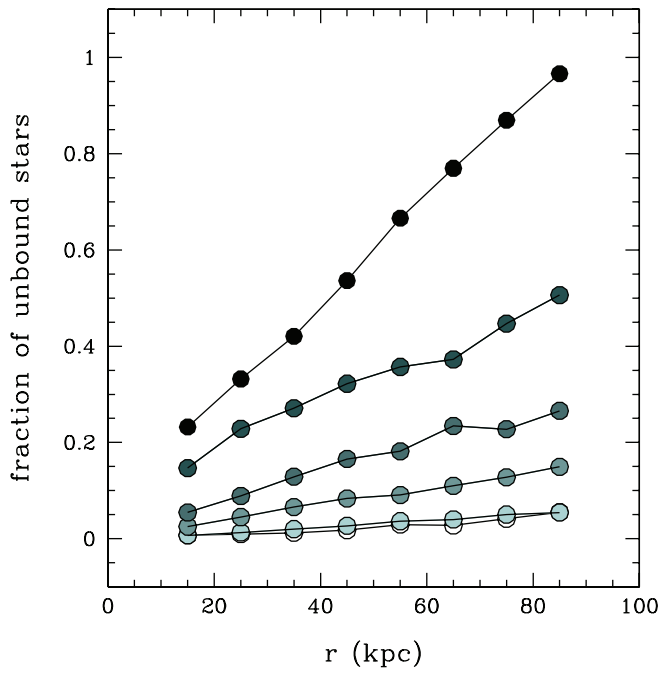

FIG. 5.—Fraction of unbound stars as a function of galactocentric distance for equal-mass binaries. The masses are the same as in Fig. 4, with 4 $M_\odot$ for the top curve and 0.6 $M_\odot$ for the bottom curve.

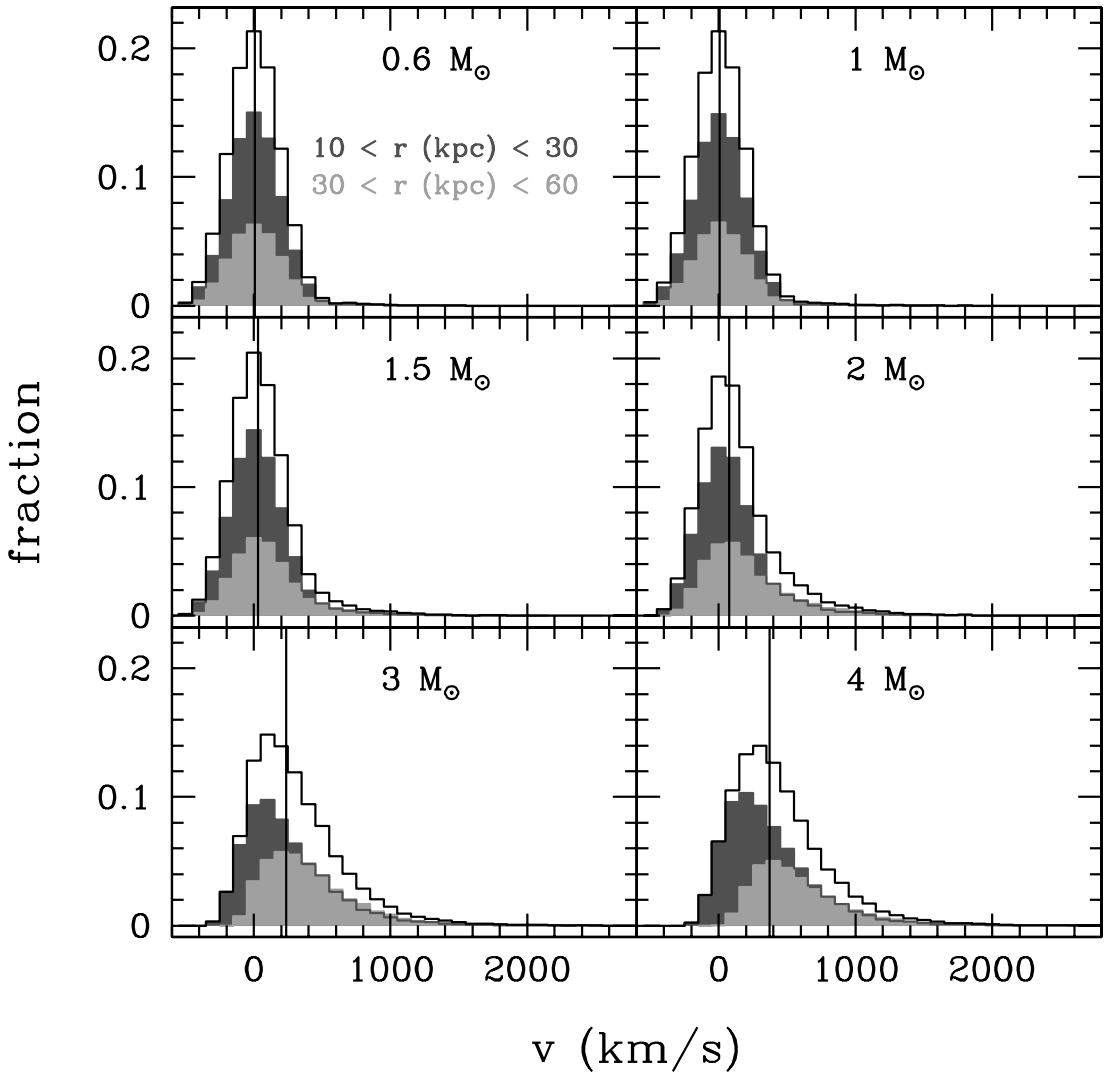

FIG. 6.—Predicted radial velocity distributions for equal-mass binaries. The gray and black histograms show the distributions in two different galactocentric distance ranges; the open histograms show results for all objects at 10–60 kpc.

have steeper density profiles. For both bound and unbound stars, low-mass stars with main-sequence lifetimes longer than the travel time from the Galactic center have shallow density profiles. Although they are typically ejected at larger velocities, many shorter-lived 3–4 $M_\odot$ stars evolve off the main sequence before reaching 50–100 kpc and thus have the steepest density profile, particularly at large r.

The large range in main-sequence lifetimes among 0.6–4 $M_\odot$ stars leads to clear differences in the fraction of unbound stars as a function of stellar mass and galactocentric distance (Fig. 5). Massive main-sequence stars observed at $r \gtrsim 50$ kpc must have relatively large ejection speeds and short travel times. Thus, most massive stars at large r are unbound. Low-mass main-sequence stars ejected on bound trajectories have much longer to reach $r \gtrsim 50$ kpc before evolving off the main sequence. Because there are more ejected stars on bound orbits than on unbound orbits, most observable ejected low-mass stars are bound at all r.

The velocity distributions of observable ejected stars are also a strong function of stellar mass (Fig. 6; Table 2). For 3–4 $M_\odot$ stars, the velocity histograms are asymmetric, with median velocities of ~400–500 km s^{-1} for stars with $r \gtrsim 30$ kpc. The median velocity is sensitive to r; nearer stars have smaller median velocities. Because the typical travel time to $r \gtrsim 30$ kpc is a significant fraction of $t_{\rm ms}$ for a 3–4 $M_\odot$ star, more massive stars must have larger ejection speeds to reach larger r. Thus, more distant regions of the halo tend to hold faster-moving ejected stars (Bromley et al. 2006).

For stars with masses $\lesssim 2$ $M_\odot$, the velocity histograms are more symmetric with decreasing stellar mass. Two physical effects produce symmetric velocity histograms for the lowest mass ejected stars: (1) most ejected stars that reach $r \gtrsim 10$ kpc are bound and (2) because 1 $M_\odot$ stars live far longer than 2–4 $M_\odot$ stars, most of the bound population consists of low-mass stars (Fig. 5). For typical $t_{\rm orb} \sim 1$ Gyr, these stars live long enough to make several orbits of the Galaxy. Bound 2–4 $M_\odot$ stars nearly always evolve off the main sequence before completing a single orbit of the Galaxy. Thus, bound stars increasingly dominate the velocity histograms of observable lower mass stars.

To illustrate the importance of the stellar lifetime in more detail, Figures 7 and 8 show the median speed as a function of galactocentric distance for the entire observable population (Fig. 7) and for outgoing observable stars only (Fig. 8). The 3–4 $M_\odot$ stars ejected at relatively small velocities ($v_0 \lesssim 700$–800 km s^{-1}; Fig. 2) do not live long enough to reach $r \gtrsim 10$ kpc. Lower mass stars live long enough for nearly all ejected stars to reach $r \gtrsim 10$ kpc. Thus, more massive stars observed at $r \gtrsim 10$ kpc move faster than

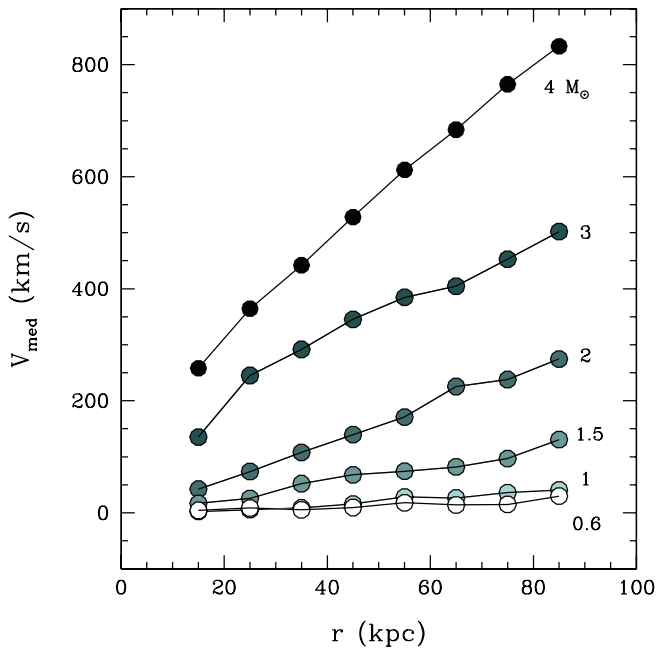

FIG. 7.—Median speed as a function of galactocentric distance for stars ejected from equal-mass binaries. The labels indicate the stellar mass; the shade of the points gets darker with mass.

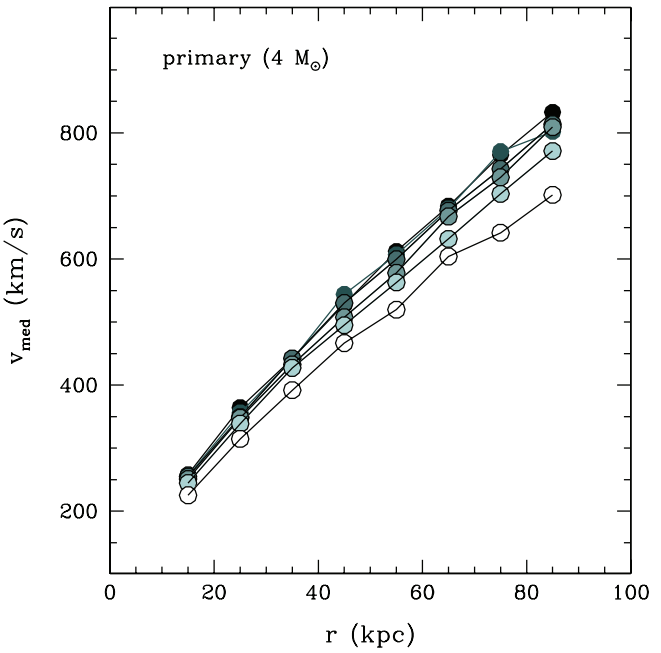

FIG. 9.—Same as Fig. 7, but for 4 $M_\odot$ primary stars in unequal-mass binaries.

lower mass stars. At even larger distances, the short stellar lifetimes of massive stars select for stars ejected at even larger velocities. Thus, the median speed of observable massive ejected stars is a strong function of r (see also Bromley et al. 2006). The longer lifetimes of low-mass stars allow a larger fraction of ejected stars to reach large r; thus, the median speed depends only weakly on r.

The median speeds of primary stars ejected from unequal-mass binaries are fairly insensitive to the mass ratio q of the disrupted binary (Fig. 9). Massive primary stars ejected from low-mass binaries tend to have somewhat smaller median speeds than massive stars ejected from more massive binaries. For binaries with 0.6 $M_\odot$ secondaries, the large mass ratio leads to the smallest ejection velocities and thus the longest travel times for the 4 $M_\odot$ primary (eq. [6]). For binaries with 1 $M_\odot$ secondaries, the longer travel times lead to smaller median speeds only for $r \gtrsim 80$ kpc, where the density profile is very steep (Fig. 4).

The median speeds of secondary stars are much more sensitive to q (Fig. 10). Although secondary stars ejected from unequal-mass binaries are ejected at larger speeds than their equal-mass counterparts (eq. [6]), two features of the ejection process lead to *smaller* median speeds for secondary stars observed at $r \sim$ 10–80 kpc (compare with Fig. 7). Because the primary stars of

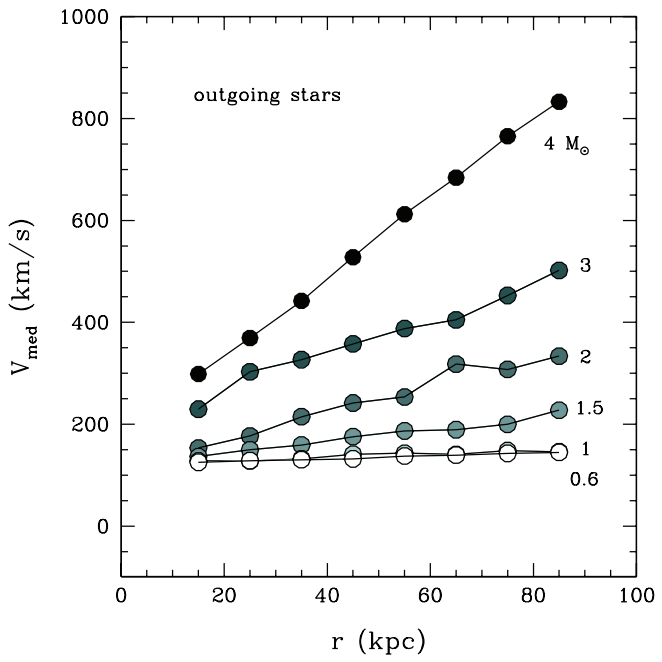

FIG. 8.—Same as Fig. 7, but for outgoing stars.

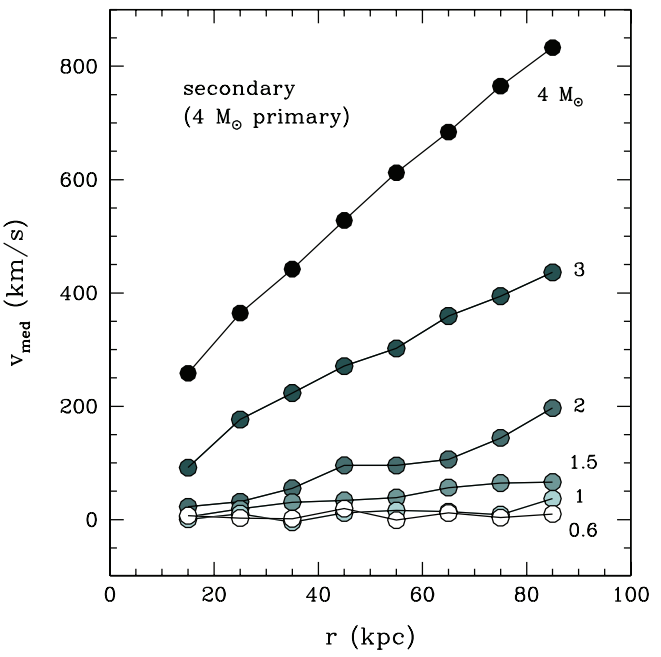

FIG. 10.—Same as Fig. 7, but for secondary stars in unequal-mass binaries with a 4 $M_\odot$ primary.

TABLE 4
MEDIAN SPEEDS OF EJECTED STARS AT 30–60 kpc

Stellar Mass ($M_\odot$)	0.6 $M_\odot$	1 $M_\odot$	1.5 $M_\odot$	2 $M_\odot$	3 $M_\odot$	4 $M_\odot$
Simple Spherical Potential						
0.6	**7**	**10**	**32**	**73**	**211**	**321**
1	5	**7**	**29**	**71**	**224**	**351**
1.5	5	3	**32**	**77**	**229**	**361**
2	5	5	19	**77**	**235**	**364**
3	1	6	15	49	**238**	**369**
4	6	3	18	39	179	**372**
Three-Component Potential from Gnedin et al. (2005)						
0.6	**5**	**4**	**21**	**42**	**135**	**234**
1	2	**4**	**19**	**44**	**137**	**238**
1.5	−1	1	**17**	**42**	**137**	**240**
2	3	−1	9	**43**	**139**	**241**
3	1	3	11	24	**135**	**242**
4	0	3	9	22	104	**240**
Three-Component Potential from This Paper						
0.6	**7**	**10**	**30**	**70**	**199**	**309**
1	6	**7**	**30**	**70**	**206**	**330**
1.5	4	3	**31**	**70**	**209**	**340**
2	6	7	17	**69**	**213**	**342**
3	1	10	16	43	**216**	**345**
4	4	4	17	39	161	**347**

NOTES.—Velocity data (in units of km s^{-1}) derived from simulations with the simple spherical Galactic potential, the three-component Galactic potential from Gnedin et al. (2005), and the three-component Galactic potential derived here. The bold entries correspond to the speed of the primary star in the binary progenitor; otherwise, the speed corresponds to the secondary star.

unequal-mass binaries have shorter lifetimes than the secondaries, the median age of an ejected secondary star is smaller for an unequal-mass binary than for an equal-mass binary. Thus, the secondary stars in unequal-mass binaries have longer median travel times. Longer travel times allow secondaries ejected at velocities larger than the median ejection velocity (eq. [2]) to reach $r \gtrsim 80$ kpc, removing these stars from the population at $r \sim 20$–80 kpc. Longer travel times also allow more slowly moving ejected stars to reach large r. Removing the highest velocity stars from the population and adding more slowly moving stars reduces the median velocities of secondaries at $r \sim 20$–80 kpc.

To summarize, simulations in the simple spherical potential yield two classes of ejected stars observable at $r \gtrsim 20$ kpc. The bound population of mostly long-lived, low-mass stars has a steep radial density profile, $\rho(r) \propto r^{-n}$ with $n \approx 3$, and a symmetric radial velocity profile centered at $v_r \approx 0$ km s^{-1} (Figs. 4–6; Table 4). Short-lived 3–4 $M_\odot$ bound stars have slightly steeper radial density profiles and provide a high-velocity tail to the radial velocity distribution at +275 to +500 km s^{-1}. Unbound ejected stars with $v \gtrsim +500$ km s^{-1} have shallow radial density profiles ($n \approx 2$–2.5). The short lifetimes of 3–4 $M_\odot$ unbound stars yield very steep density profiles at large radii ($n \gtrsim 3$ for $r \gtrsim 80$ kpc). Thus, the relative frequency of 3–4 $M_\odot$ unbound stars decreases relative to lower mass unbound stars at $r \gtrsim 80$ kpc.

4. OBSERVABLE EJECTED STARS IN A THREE-COMPONENT GALAXY

We now consider the evolution of observable ejected stars in a three-component potential consisting of a bulge, disk, and halo (eq. [10]). We discuss results for the Gnedin et al. (2005) Galaxy model, which has a relatively small acceleration at small r, and for our three-component model Galaxy, which has a larger acceleration at small r. The acceleration at small r for our model Galaxy is comparable to the acceleration for the simple spherical potential (§ 2.2; Fig. 1). To minimize differences in median velocities caused by the relatively massive disk in our model Galaxy, we derive results for ejections along the z-axis. To minimize the number of low-velocity stars ejected into the halo of the Gnedin et al. (2005) model Galaxy, we derive results for ejections in the disk plane, where the larger deceleration from the disk prevents more low-velocity ejected stars from reaching 10 kpc.

At 10–60 kpc, the velocity histograms derived for ejections into our model Galaxy and the simple spherical Galaxy are indistinguishable (Fig. 11). In both cases, the distributions for 4 $M_\odot$ stars are greatly skewed to large velocities, with more low-velocity stars at 10–30 kpc than at 30–60 kpc. These models yield a small ($\sim$10%) fraction of stars returning to the Galactic center with negative velocities. For 0.6 $M_\odot$ stars, the distributions are nearly symmetric about zero velocity, consistent with a large population of bound stars in both examples. In addition to a modest fraction ($\sim$10%) of unbound stars, models for 0.6 $M_\odot$ stars have a large fraction ($\sim$45%) of returning stars.

At 10–60 kpc, calculations with the Gnedin et al. (2005) Galaxy potential yield more symmetric velocity histograms and many fewer unbound stars than calculations using the other Galaxy models. For 2–4 $M_\odot$ stars, the velocity histograms are skewed to high velocities but have a smaller fraction of stars with velocities exceeding 600–800 km s^{-1} (Fig. 11). Ejections into this potential also produce a much larger population of stars at 10–30 kpc than at 30–60 kpc. For lower mass stars, the velocity histograms are more similar to those derived from the other Galaxy models. However, velocity histograms with this potential have smaller dispersions about the median velocity.

Table 4 compares median speeds at 30–60 kpc for the three Galaxy models. For 2–4 $M_\odot$ primary and secondary stars, the median speeds derived for our three-component Galaxy are $\sim$5%–15% smaller than those derived for the simple spherical Galaxy. This difference results from the potential at $r \sim 1$ kpc, where the three-component potential produces a smaller acceleration than the simple potential (Fig. 1). The median speeds of massive stars in the Gnedin et al. (2005) potential are typically $\sim$75% of those for the other potentials. For 0.6–1 $M_\odot$ stars, the median speeds derived for the three models are similar. Although the median velocities of low-mass stars in the Gnedin et al. (2005) potential are approximately two-thirds of the median velocities derived for the other potentials, the typical difference of 6–12 km s^{-1} is small compared to current observational errors.

In these calculations, the large differences between the median speeds and the shapes of the velocity histograms are set by the Milky Way potential at $r = 5$–200 pc (Fig. 1). At small r, the potential acts as a high-pass filter, preventing low-velocity stars from reaching the halo (Fig. 2). In the Gnedin et al. (2005) potential, lower velocity stars reach the halo. Thus, the median speeds of observable stars are smaller and the velocity histograms are narrower. In the simple spherical Galaxy and our three-component Galaxy, low-velocity stars are trapped at $r \lesssim 10$ kpc. Thus, the median speeds are larger at all $r \gtrsim 10$–20 kpc. Because low-velocity bound stars remain at $r \lesssim 10$ kpc in our three-component Galaxy, the velocity histograms of these stars are also broader for all $r \gtrsim 10$–20 kpc.

Because the potential of the central 200 pc of the Galaxy makes such a large difference in the median speeds of observable HVSs at 10–60 kpc, our results suggest that HVSs might be a

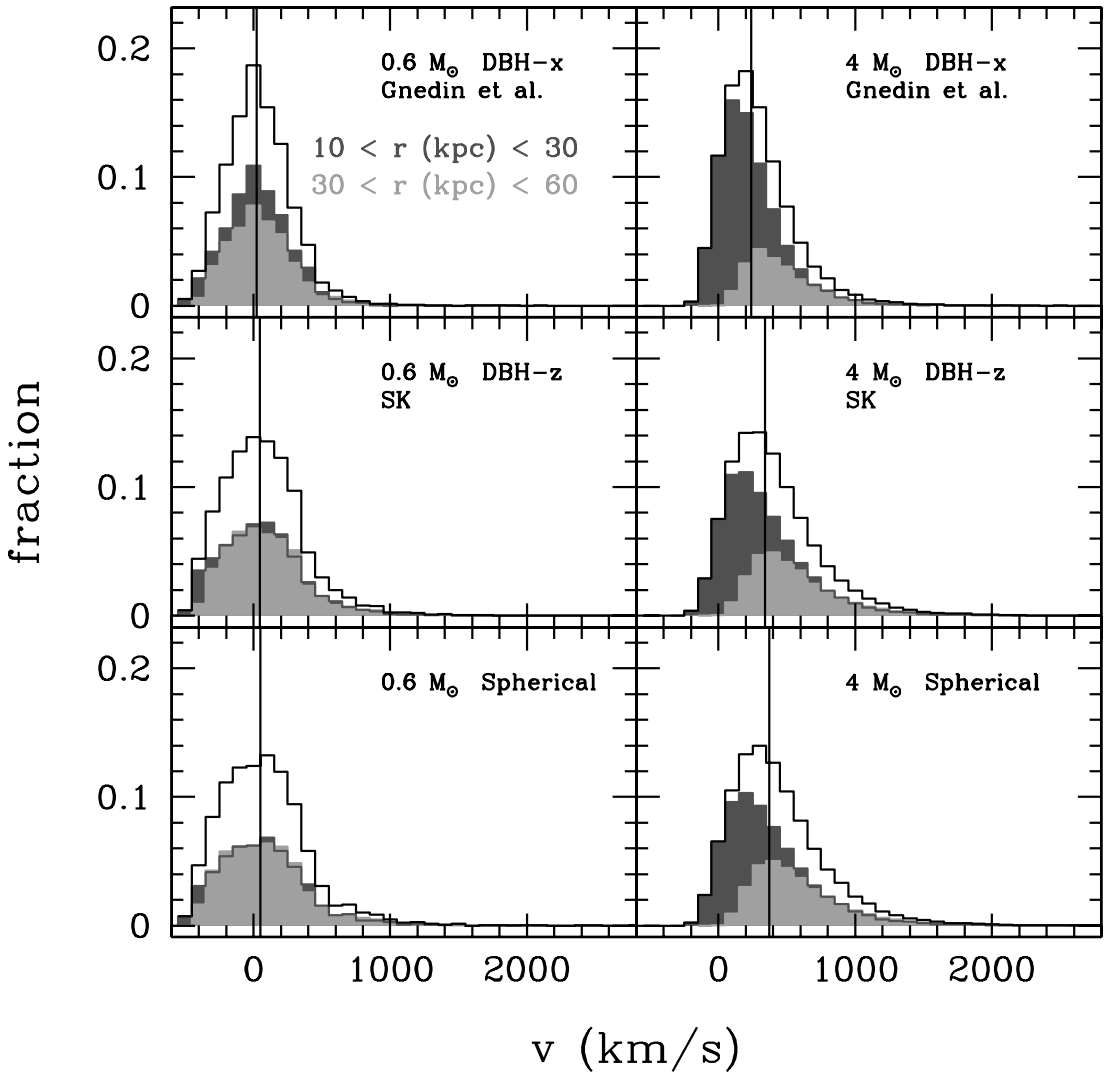

FIG. 11.— Same as Fig. 6, but for stars in the three-component and spherical Galaxy potentials. *Top panels*: Velocity histograms in the plane of the disk in the Gnedin et al. (2005) potential for 0.6 $M_\odot$ stars (*left*) and 4 $M_\odot$ stars. *Middle panels*: Same as top panels, but for ejections along the z-axis of our three-component potential. *Bottom panels*: Same as top panels, but for the simple spherical potential of Fig. 6.

useful probe of the triaxial potential of the central Galaxy. To test this possibility, we consider two triaxial models for the inner Galaxy. Stolte et al. (2008) analyze the mass density data of Launhardt et al. (2002) and derive a three-component triaxial model for the central 200 pc. Each component in this model has axial ratios $x_0 : y_0 : z_0$. With a minimum axial ratio of 0.71 in the z-direction (for the nuclear stellar disk), we predict an expected reduction of 15–20 km s^{-1} in the median speeds of stars ejected along the z-axis relative to stars ejected in the plane of the Galaxy. Using OGLE data for the bulge, Rattenbury et al. (2007) derive a triaxial model for the Galactic bar with $x_0 : y_0 : z_0 = 1.0 : 0.35 : 0.26$. Assuming that the rotation of the bar eliminates any signal in HVS speeds along the y-axis, we expect a reduction of 25–30 km s^{-1} in the median speeds of HVSs ejected along the z-axis of the bar relative to those ejected in the Galactic plane.

Given the current uncertainties in mass models for the Galaxy, our simulations suggest that the radial density profiles and velocity histograms of HVSs at $r \gtrsim 20$ kpc are most sensitive to the form of the Galactic potential for $r \lesssim 0.1$–1 kpc. At $r \gtrsim 1$ kpc, small changes to the potential produce negligible differences in observable quantities. At $r \lesssim 200$ pc, triaxial potentials consistent with observations produce $\pm$10–30 km s^{-1} differences in the median velocities of observable unbound stars as a function of Galactic latitude and negligible differences in the radial density profiles. These differences are comparable to the variation in median speeds among 0.6–1.5 $M_\odot$ ejected stars, where the shorter stellar lifetimes of more massive stars produce median speeds offset from $v_r \approx 0$. With high-quality stellar mass estimates, HVSs could provide constraints on the triaxiality of the central Galactic potential.

5. SCALED DENSITY PROFILES AND SEARCHES FOR HVSs

The Hills (1988) ejection mechanism for HVSs has several observable consequences. In Bromley et al. (2006) and in this paper, we show that radial velocity surveys for massive main-sequence stars should reveal comparable numbers of bound and unbound HVSs. Our results also suggest that 4 $M_\odot$ HVSs should have smaller space densities at $r \sim 50$–100 kpc than 3 $M_\odot$ HVSs. Observations confirm both predictions. Brown et al. (2007a, 2007b) identify 26 bound B-type HVSs with $v_r \gtrsim 275$ km s^{-1} and only 1 bound HVS with $v_r \lesssim -275$ km s^{-1}, supporting the notion that the B-type HVSs are main-sequence stars and not horizontal-branch stars. In these data, longer-lived 3 $M_\odot$ HVSs

fill the survey volume out to $r \sim 80$–90 kpc; shorter-lived 4 $M_\odot$ HVSs are missing at large distances. This result confirms our expectation that stellar lifetimes set the HVS space density at large r.

From an analytic analysis of the radial density profiles of unbound stars, Kollmeier & Gould (2007) develop a strong motivation to search for HVSs among 0.6–1 $M_\odot$ stars. They conclude that a survey of faint stars near the main-sequence turnoff might yield as many as 0.022 HVSs deg^{-2}, roughly a factor of 20 larger than the $\sim$0.001 HVSs deg^{-2} inferred from our targeted survey of B-type stars (Brown et al. 2007b). Our calculations in §§ 3 and 4 suggest that the large bound population of observable ejected turnoff stars overwhelms the unbound component, especially at $r \sim 10$–40 kpc, where the radial velocities of turnoff stars can be measured with existing multiobject spectrographs (Fig. 6). However, if the relative space density of bound, low-mass ejected stars is large enough relative to the indigenous halo population, fruitful searches for low-mass HVSs might still be possible (see Kollmeier & Gould 2007). The success of the HVS ejection model for 3–4 $M_\odot$ stars and the Kollmeier & Gould (2007) suggestion leads us to take a more detailed look at the likelihood of identifying large samples of HVSs among lower mass stars.

5.1. *Relative Space Densities as a Function of Stellar Mass*

To quantify the relative space densities of HVSs as a function of stellar mass in our simulations, we must scale the density profiles in Figure 4. For each stellar mass, we require the relative frequency of primary and secondary stars as a function of stellar mass (the mass function), the relative frequency of binaries with the range of separations ($a_{\rm min}$, $a_{\rm max}$), and an efficiency factor relating the number of stars ejected from the Galactic center to the number observed at $r \approx 10$–100 kpc. For simplicity, we assume that the binary frequency is independent of primary mass and that the mass function is independent of orbital separation. Although observations suggest the binary frequency depends on stellar mass (e.g., Lada 2006), the differences in binary frequencies among nearby 0.6–4 $M_\odot$ stars are small compared to uncertainties in the mass function and the relative frequency of binary separations.

To construct a first estimate of the scaled density profiles of unbound stars as a function of stellar mass, we develop a simple model. For each stellar mass m, we derive a weighting factor

$$x(m) = x_1(m)x_2(m, a)x_3(m)t_{\rm ms}, \tag{12}$$

where $x_1(m)$ is the relative number of stars of mass m, $x_2(m, a)$ is the relative number of binary stars with orbital separations in the range $a_{\rm bin} = (a_{\rm min}, a_{\rm max})$, and $x_3(m)$ is the relative fraction of stars ejected from 1.45 pc that reach $r \gtrsim 10$ kpc. To account for stellar evolution, we scale the weighting factor by the main-sequence lifetime $t_{\rm ms}$ in Table 1. We set $x(m = 0.6\ M_\odot) = 1$ and normalize other weights accordingly. This model assumes that primary and secondary stars are selected from the same mass function, a reasonable first approximation.

To derive x_1, we adopt a simple power-law mass function

$$\xi(m)dm \propto m^{-(q+1)}dm, \tag{13}$$

where $q \approx 1$–1.5 (e.g., Salpeter 1955; Miller & Scalo 1979). Integrating this function over m yields relative numbers of stars in mass ranges with lower mass limits m_l and upper mass limits m_u. For a set of stellar masses, $S(m) = \{0.6, 1.0, 1.5, 2.0, 3.0, 4.0\}$, we choose a set of lower mass limits $S(m_l) = \{0.4, 0.8, 1.25, 1.75, 2.5, 3.5\}$ and a set of upper mass limits $S(m_u) = \{0.8, 1.25, 1.75, 2.5, 3.5, 4.5\}$.

To guide our choices for the exponent q, we rely on recent observations of the Arches cluster near the Galactic center (Stolte et al. 2005; Kim et al. 2006). These analyses suggest a current mass function with $q \approx 0.9$, top-heavy compared to the local Salpeter mass function with $n \approx 1.35$. However, dynamical interactions among cluster stars may produce mass segregation on timescales comparable to the cluster age, flattening the mass function in the core and steepening it in the outskirts of the cluster (Dib et al. 2007; Portegies Zwart et al. 2007). Thus, the most likely exponent for Arches stars is probably $q \approx 1.0$–1.35. To provide estimates for a range of q, we derive $S(x_1) = \{1.0, 0.29, 0.13, 0.086, 0.05, 0.025\}$ for $q = 1.35$ and $S(x_1) = \{1.0, 0.36, 0.18, 0.14, 0.09, 0.05\}$ for $q = 1.0$.

Observations of the Arches cluster and other young stars currently provide no constraints on the frequency of separations for close binaries in the Galactic center. To derive x_2, we thus rely on observations in the local solar neighborhood. For nearby binaries with A-type and B-type primary stars, $a_{\rm bin}$ is distributed with roughly equal likelihood per logarithmic interval (Abt 1983; Heacox 1998). For stars with orbital separations in the range $a_{\rm bin} = (a_{\rm min}, a_{\rm max})$ from Table 1, this assumption yields a set of values for x_2, $S_1(x_2) = \{1.0, 0.66, 0.45, 0.41, 0.39, 0.39\}$.

For nearby solar-type stars, the frequency of binary separations is closer to a lognormal distribution (Duquennoy & Mayor 1991). For this relation, we derive $S_2(x_2) = \{1.0, 0.95, 0.90, 0.87, 0.86, 0.85\}$. Because this frequency distribution underweights binaries with small separations, it underweights low-mass ejected stars relative to massive ejected stars. To maximize the predicted relative density of low-mass stars, we adopt the S_1 set of weights for x_2. This decision may overestimate the relative abundance of solar-type stars[4] by a factor of $\sim$2.

To derive x_3, we rely on the calculations for §§ 3 and 4. For a complete derivation of x_3, we require a full set of simulations spanning the entire range of binary separations and mass functions for primary and secondary stars. Because very few binaries produce ejected stars, this simulation requires a significant computational effort for little return. In the set of simulations made for this paper, the ratio of failed to successful ejections is nearly independent of the masses of the primary and secondary stars and the initial binary separation. Thus, for our first estimate of x, we adopt $x_3 = 1$.

Figure 12 shows the scaled relative density profiles of observable main-sequence stars from this simple model. For clarity, we normalize the density profiles for 1–4 $M_\odot$ stars to the density profiles for 0.6 $M_\odot$ stars. Thus, the relative densities of 0.6 $M_\odot$ stars are unity at all r. For all 0.6–4 $M_\odot$ ejected stars (*top panels*), the density profiles scale inversely with stellar mass. Thus, low-mass ejected stars are relatively more abundant than massive stars at all r. Because shallower mass functions contain relatively more massive stars, the differences in the scaled density profiles are smaller for smaller n. For unbound 1–4 $M_\odot$ stars at $r \sim 10$–200 kpc, the density profiles are roughly constant with r and scale inversely with stellar mass (*bottom panels*). Aside from the dramatic decline in the relative density of 4 $M_\odot$ stars at $r \gtrsim 30$ kpc due to their relatively short main-sequence lifetimes, massive unbound stars are a factor of $\sim$10 less abundant than low-mass unbound stars at all r.

[4] Other physical processes, including binary evaporation near the MBH (Perets 2007) and interactions between binaries and molecular clouds (Perets et al. 2007), can lower the relative abundance of solar-type stars among HVSs. To maximize the predicted density of low-mass stars among HVSs, we ignore these processes in our estimate of x_2.

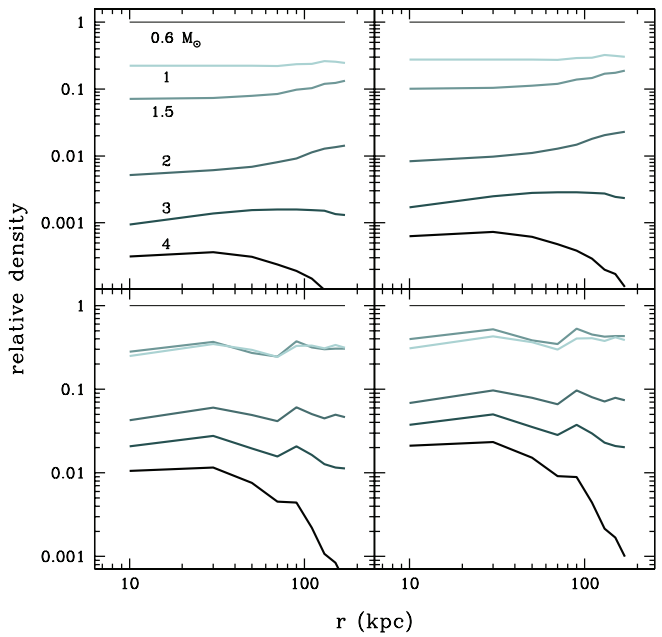

FIG. 12.—Relative density profiles for HVSs as a function of stellar mass. In all panels, we normalize the density profiles for 0.6 $M_\odot$ stars to unity at all r. *Top panels*: Profiles for all ejected stars for mass functions with $q = -1.35$ (*left*) and $q = -1$ (*right*). *Bottom panels*: Same as top panels for unbound stars. Compared to a population of 0.6–1 $M_\odot$ ejected stars, the relative abundance of more massive ejected stars declines monotonically with stellar mass (*top panels*). For unbound stars (*bottom panels*), 3–4 $M_\odot$ (1.5–3 $M_\odot$) stars are relatively more abundant than 0.6–1 $M_\odot$ stars at $r \lesssim 50$–80 AU ($r \gtrsim 80$–100 AU). Although these results show that 2–4 $M_\odot$ ejected stars are factors of 10–100 less numerous than 0.6–1 $M_\odot$ ejected stars, magnitude-limited surveys for HVSs are likely to yield comparable numbers of massive ejected stars (see Table 5).

Two physical effects cause the changes in the slopes of the scaled density profiles in Figure 12. Because massive ejected stars contain a larger fraction of unbound stars (Fig. 4), massive ejected stars have shallower density profiles at small r than low-mass ejected stars. Thus, the scaled density profiles for massive stars rise with r. At large r, however, short stellar lifetimes remove massive stars from the sample of observable unbound stars. For 4 $M_\odot$ stars, the typical travel time to $r \sim 50$–100 kpc is comparable to the main-sequence lifetime, $t_{\rm ms} \approx 160$ Myr (Table 1). Thus, the relative densities of 4 $M_\odot$ stars decline considerably at $r \sim 50$–100 kpc. For 2–3 $M_\odot$ stars, the typical travel time to $r \sim 50$–100 kpc is less than half of the main-sequence lifetime, $t_{\rm ms} \approx 300$ Myr to 1 Gyr. Thus, the relative densities for these stars decline with r less dramatically than the relative densities for massive stars.

The relative numbers of bound stars as a function of stellar mass depend primarily on the mass function and the relative stellar lifetimes (eq. [12]). For a mass function with $q = 1.35$ and the stellar lifetimes in Table 1, the relative number of 0.6 and 3 $M_\odot$ stars is $\sim$800:1, close to the prediction of $\sim$1000:1 from the detailed model.

In contrast, the relative numbers of unbound stars are nearly independent of stellar lifetime. Because the time for unbound stars to reach $r \sim 50$–100 kpc is a small fraction of the main-sequence lifetimes for 0.6–2 $M_\odot$ stars, the relative numbers of 0.6–2 $M_\odot$ unbound stars depend primarily on the adopted mass function. Thus, for $q = 1.35$, the relative number of 0.6 and 2 $M_\odot$ unbound stars is $\sim$12:1. For more massive stars, the travel time is comparable to the main-sequence lifetime. If we assume that $\sim$50% of 3–4 $M_\odot$ stars evolve off the main sequence as they travel from 10 to 100 kpc, the relative numbers of 0.6 and 3–4 $M_\odot$ unbound stars is $\sim$50:1 for a mass function with $q = 1.35$, close to the prediction in Figure 12.

TABLE 5
RELATIVE NUMBERS OF EJECTED STARS

Mass ($M_\odot$) (1)	M_V (2)	$n_{e,21}$ (3)	$n_{e,23}$ (4)	$n_{u,21}$ (5)	$n_{u,23}$ (6)
0.6	8.3	160	400	8	16
1.0	5.0	125	300	6	20
1.5	3.1	55	110	5	20
2.0	1.7	30	70	8	15
3.0	−0.3	15	15	4	4
4.0	−0.9	1	1	1	1

NOTE.—These parameters are described in § 5.

5.2. *Predicted Detections*

Converting the relative density profiles of Figure 12 into predicted detection rates requires a targeting strategy. We follow Brown et al. (2006a) and assume that target stars are selected from a magnitude-limited survey. For simplicity, we consider a shallow magnitude-limited survey to $V_{\rm max} = 21$ and a deeper survey to $V_{\rm max} = 23$. To estimate relative detection rates, we derive absolute V magnitudes as a function of stellar mass using the Schaller et al. (1992) and Schaerer et al. (1993) evolutionary tracks and bolometric corrections from Kenyon & Hartmann (1995). We use these estimates to derive the maximum observable distance, $r_{\rm max}(m, V_{\rm max})$, for each stellar mass in our set of masses. Integrating the relative densities in Figure 12 over the distance from $r = 8$ kpc to $r_{\rm max}(m, V_{\rm max})$ then yields the relative numbers of stars of each mass as a function of $V_{\rm max}$. For surveys that yield one observable 4 $M_\odot$ HVS, we predict $n_{e,m}$, the relative number of observable ejected stars at mass m, and $n_{u,m}$, the number of observable unbound stars at mass m. Table 5 lists our results.

Shallow surveys with $V_{\rm max} \leq 21$ are sensitive to HVSs of all masses (see cols. [3] and [5] of Table 5). Roughly 40% (12%) of the unbound (bound) ejected stars are 2–4 $M_\odot$ stars with $M_V = +1.7$ to -1. Because lower mass stars have longer main-sequence lifetimes, these stars comprise a larger fraction of bound stars in a magnitude-limited survey. Nearly all ($\sim$94%) observable ejected stars with $m \approx 0.6$–1.5 $M_\odot$ are bound to the Galaxy. However, $\sim$25% of ejected 2–4 $M_\odot$ stars are unbound. Thus, shallow surveys targeting 2–4 $M_\odot$ stars have a higher probability of observing unbound HVSs than surveys for lower mass stars.

Deeper surveys with $V_{\rm max} = 23$ yield larger fractions of lower mass stars in the bound and unbound populations (see cols. [4] and [6] of Table 5). Although our analysis predicts that $\sim$50% (75%) of the unbound (bound) ejected stars with $V \leq 23$ are 0.6–1 $M_\odot$ stars, only $\sim$5% of observable low-mass ejected stars are unbound. Among 1.5–4 $M_\odot$ stars, we derive a much larger fraction of unbound stars, $\sim$25%. Because 3–4 $M_\odot$ unbound stars are relatively rare in surveys with $V_{\rm max} = 23$, deep surveys targeting 1.5–2 $M_\odot$ stars have the highest probability of detecting unbound HVSs.

Several competing physical effects combine to produce the results in Table 5. Massive stars are much brighter than low-mass stars; thus, magnitude-limited surveys probe much larger volumes for massive stars than for low-mass stars. For typical density profiles $\rho \propto r^{-2}$, the relative numbers of stars scale with their limiting distances $r_{\rm max}$ (see also Kollmeier & Gould 2007).

All unbound stars spend comparable times traveling from 10 to 200 kpc. Thus, the relative numbers of unbound stars scale with the mass function at the Galactic center, $r_{\rm max}$, and the ratio of travel time to stellar lifetime. For 1 and 3 $M_\odot$ stars, these factors yield relative numbers of 6:1 (mass function), 1:10 ($r_{\rm max}$), and 2:1 (stellar lifetimes); the simple estimate for the relative number of $\sim$1:1 is close to the tabulated values.

To make a simple estimate for the relative numbers of bound stars, we need a larger correction for relative stellar lifetimes. Because low-mass stars live longer than the typical orbital time of $\sim$1 Gyr, the bound population samples low-mass stars ejected throughout the lifetime of the Galaxy. For 1 and 3 $M_\odot$ stars, the relative stellar lifetimes ($\sim$30:1) yield relative numbers of 15:1 in a magnitude-limited survey, close to the tabulated values of 10–20:1. Thus, as Kollmeier & Gould (2007) first pointed out, low-mass bound stars dominate the population of observable ejected stars in all magnitude-limited surveys.

As a final piece of this analysis, we consider identifying HVSs within the large population of indigenous halo stars. Brown et al. (2006a) use SDSS $(g' - r')_0$ and $(u' - g')_0$ colors to target 3–4 $M_\odot$ HVSs with $g'_0 \lesssim 19.5$. Searching for massive stars in this color-magnitude space has several advantages over searches for lower mass HVSs: (1) surveys for bright, massive HVSs sample a large volume; (2) the predicted fraction of unbound stars is $\sim$50% (Fig. 4); (3) the predicted velocity histogram for bound stars is more asymmetric (Fig. 6), and thus they are more readily detectable; and (4) two colors reduce white dwarf and quasar contamination considerably, yielding a 3 $M_\odot$ HVS candidate list of manageable size (see also Brown et al. 2007a, 2007b).

In a 6800 deg^2 survey of 575 candidates with $17.0 < g'_0 < 19.5$, Brown et al. (2007b) identify seven unbound HVSs and nine probable bound HVSs. The surface number density of unbound 3 $M_\odot$ HVSs is $\sim$0.001 deg^{-2}; the surface number density of observed 3 $M_\odot$ ejected stars is $\sim$0.002 deg^{-2}. In this shallow survey, the relative numbers of bound and unbound HVSs agree well with model predictions (Brown et al. 2007b). The survey detection efficiency (number of HVSs detected divided by number of candidates) is 1.2% for unbound objects.

At the other end of the mass range we explore in Table 5, Kollmeier & Gould (2007) propose observing fainter ($19.5 < g' < 21.5$) stars near the main-sequence turnoff with masses $m \approx 0.8$–1.3 $M_\odot$. Applying scaling arguments to the Brown et al. (2006a) detections, Kollmeier & Gould (2007) predict one turnoff HVS per 45 deg^2 within their suggested survey limits. These arguments, and a later corroborating estimate by Brown et al. (2007b), assume that the velocity distribution of HVSs is independent of their mass, contrary to the more detailed calculations for Table 5.

However, Kollmeier & Gould (2007) scale the relative numbers of massive HVSs by the present-day mass function, which is a product of the initial mass function (IMF) and stellar evolution.[5] This approach is valid for the bound population. Thus, the predictions of one turnoff HVS per 45–50 deg^2 (Kollmeier & Gould 2007; Brown et al. 2007b) are reasonable estimates for the bound population of low-mass HVSs. Because all unbound stars spend roughly equal amounts of time traveling through the halo, the relative numbers of unbound stars scale with the IMF. This scaling reduces the predicted sky surface density of unbound low-mass HVSs relative to unbound massive HVSs as outlined above. Thus, Kollmeier & Gould (2007) overestimate the detectable population of unbound HVSs by a factor of $\sim$30–100. Unbound stars are a small fraction of the observable ejected turnoff stars.

According to Table 5, $\sim$5% of turnoff stars in a survey for low-mass HVSs with $g'_0 \leq 21.5$ are unbound. Within the more dominant bound population, $\sim$20% should have $|v| \gtrsim 275$ km s^{-1}. For a predicted sky surface density of one bound HVS per 45–50 deg^2, detecting unbound or bound low-mass HVSs within a larger (300 stars deg^{-2}) population of indigenous halo stars may be challenging. Detecting a single unbound low-mass HVS requires observations of $\sim 3 \times 10^5$ stars. This large sample would yield approximately five bound candidates with $|v| \gtrsim 275$ km s^{-1}. We emphasize that only the signature of an unbound HVS is unambiguous; the bound component may be difficult to distinguish from the well-populated tails of the velocity distribution of the indigenous population.

These estimates are sensitive to the ejection model for HVSs and to the adopted mass function and the fraction of stars in binaries with separations ($a_{\rm min}$, $a_{\rm max}$) in our model (x_1 and x_2 in eq. [12]). As outlined above, both of these inputs to our model are uncertain.

Nonetheless, these models indicate that identification of HVSs is increasingly difficult as the mass of the star decreases. The drivers of this conclusion are that (1) in a magnitude-limited survey massive stars are visible to greater depth, (2) the fraction of unbound stars increases with mass, (3) the velocity distributions are increasingly symmetric for less massive HVSs, and (4) the indigenous contamination increases with decreasing stellar mass.

If HVSs are ejected by a binary MBH instead of a single MBH, we expect different scaling laws with stellar mass (e.g., Sesana et al. 2006, 2007a). Clearly, for the Hills (1988) mechanism, the properties of binaries in the Galactic center are important; they are irrelevant for ejection by a binary MBH. Thus, searches for low-mass HVSs provide tests of basic inputs to our estimates for the Hills (1988) ejection mechanism, as well as the overall picture for the origin of HVSs (e.g., Perets 2007).

5.3. *Post-Main-Sequence HVSs*

Although our results indicate that low-mass main-sequence stars are not prime targets for dedicated HVS surveys, we must consider whether their post-main-sequence descendants, horizontal-branch (HB) and red giant branch (RGB) stars, are more favorable targets. HB stars are as luminous as 2–4 $M_\odot$ main-sequence stars and are thus observable to larger distances than their 1–2 $M_\odot$ progenitors (see Brown et al. 2007b). With larger luminosities than HB stars, RGB stars are also reasonable targets for HVS surveys.

To quantify the probabilities for detecting HB or RGB HVSs, we derive $r_{\rm max}(m, V)$ from adopted absolute magnitudes and lifetimes. For HB stars, we adopt $M_V \approx 0.5$ (Brown et al. 2008) and lifetimes of $\sim$1% of the main-sequence lifetime (Yi et al. 2001). Scaling the relative numbers by the relative lifetimes (a factor of 0.01) and the relative volumes (a factor of 7–8), the HB descendants of 1–2 $M_\odot$ main-sequence stars are a factor of $\sim$10 less abundant than their main-sequence progenitors. Thus, HB stars are unlikely to provide many HVSs in a deep survey.

For RGB stars, we consider deep optical and near-infrared (IR) surveys. We adopt an absolute brightness at the tip of the RGB ($M_V \approx -1.5$, $M_K \approx -6$; Bellazzini et al. 2001) and a typical lifetime of 10 Myr (Yi et al. 2001). For optical surveys with limiting magnitudes $V \leq 21$–23, we predict that RGB stars are $\sim$2% as abundant as 1–2 $M_\odot$ main-sequence stars. In an IR survey with a depth of $K = 15$ (e.g., 2MASS; Skrutskie et al. 2006), we predict that RGB stars are $\lesssim$1% as abundant as 1–2 $M_\odot$ main-sequence stars in a deep optical survey. Although RGB stars are

[5] Formally, we derive a crude estimate of the present-day relative mass function as $x_1(m)t_{\rm ms}$ in eq. (12).

observable to distances of 100–200 kpc in deep IR and optical surveys, their short lifetimes preclude detection as HVSs.

6. CONCLUSIONS

HVSs are a fascinating newly discovered class of objects because they connect the Galactic center with the outer halo of the Milky Way. We explore these connections by using the Hills (1988) model to inject stars into the Galactic potential. We track the journeys of these ejected stars across the Galaxy and derive simulated catalogs of observable HVSs.

The foundation for our model includes the construction of forms for the Galactic potential which fit observations over the range 5–10^5 pc. We demonstrate that potentials which match the observations within the central 200 pc of the Galaxy are crucial for understanding HVSs. Our approximations to the potential may be useful for other astrophysical problems which connect the central regions of the Galaxy to its outer reaches.

We show that important aspects of the median speeds and shapes of the observable velocity distributions of HVSs are set by the Milky Way potential at $r \lesssim 200$ pc. For the potentials we construct to match the observations in this central region, median speeds are larger and velocity histograms are broader. Thus, low-velocity ejected stars have less penetration into the outer halo at every stellar mass. These results indicate that HVSs might be useful probes of the triaxial potential of the central Galaxy.

The models predict the spatial and velocity distributions of observable HVSs. They also provide a physical understanding of the origin of the dependences of these distributions on stellar mass for $m = 0.6$–$4\ M_\odot$ and on distance in the halo for $r =$ 10–200 kpc. Here, we enumerate the main predictions of the model. We concentrate on the predictions resulting from our model potentials which match observations in the Galactic center. For all of these issues, we consider the subtle effects on unequal-mass binaries in the text (§ 3); here, we focus on the results for equal-mass binaries.

1. *Stellar evolution* affects the observability of HVSs. It removes them at large radii where the travel time from the Galactic center exceeds the stellar lifetime. Because the lifetimes of low-mass stars are long, the observable properties of low-mass HVSs depend only on the potential and the properties of binaries at the Galactic center.

2. For 3–4 $M_\odot$ ejected stars, the fraction of unbound HVSs increases dramatically with r in the Galactic halo (Fig. 5). Because the travel time from the Galactic center is a significant fraction of the main-sequence lifetime for these stars, the median *stellar age* of 3–4 $M_\odot$ HVSs increases monotonically with r.

In contrast, bound stars dominate the population of long-lived, low-mass HVSs. Thus, the median stellar ages are essentially independent of r.

3. The *velocity distribution* of 3–4 $M_\odot$ HVSs is asymmetric, with a long tail toward positive velocities. The shape of the velocity distribution again reflects the coincidence of stellar lifetimes and travel times. The velocity distributions of HVSs are increasingly symmetric with decreasing stellar mass.

4. As emphasized by Bromley et al. (2006), the short lifetimes of 3–4 $M_\odot$ HVSs require that they be injected with large velocities to reach the outer halo. Thus, the *median speed* of massive HVSs increases with r.

For low-mass stars, the median speed depends only weakly on r. For all stars, the median speed increases with stellar mass at fixed r.

5. The *density profiles* of unbound HVSs are approximately $\rho \propto r^{-n}$, where $n = 2$–2.5. For the most massive stars, their finite lifetime removes stars at large r, steepening the density profile ($n \gtrsim 3$ at $r \gtrsim 80$ kpc).

The density profile for bound, mostly low-mass HVSs is roughly $\rho \propto r^{-3}$. We compute the detailed behavior of these profiles (Fig. 4).

6. *Scaled density profiles* show that the relative numbers of observable unbound HVSs as a function of stellar mass are relatively independent of the stellar lifetime. They depend mostly on the mass function at the Galactic center at the time of ejection. In contrast, the relative numbers of bound HVSs are a function of the stellar lifetimes and the mass function.

7. We predict the *relative observable numbers* as a function of stellar mass for the range 0.6–4 $M_\odot$. In a magnitude-limited survey, the main factors that set detectability are (1) the accessible volume, (2) the fraction of unbound HVSs, (3) the asymmetry of the velocity distribution, and (4) contamination by indigenous stellar populations. Detection of HVSs is increasingly difficult with decreasing mass because all of these issues become less and less favorable.

We also argue that post-main-sequence stars are poor targets because their detectability is subject to yet another limit, the very short lifetimes of these phases.

Samples of HVSs which are sufficiently large to explore these predictions provide a strong test of the model for injection of the stars into the Galactic potential. Coupled with observations of the stellar population at the Galactic center, observations of HVSs provide promising probes of the binary population, the stellar mass function, and the central potential of the Milky Way (see also Perets 2007).

So far, the observations by Brown et al. (2007b and references therein) indicate that there are ~100 detectable HVSs with $m \approx$ 3–4 $M_\odot$. Detection of comparable lower mass populations may be feasible. Samples of hundreds of HVSs promise strong tests of models like the one we construct.

We thank J. Dubinski for helpful discussion on models for the Galactic potential and O. Gnedin and H. Perets for helpful comments on the manuscript. We acknowledge support from the NASA Astrophysics Theory Program through grant NAG5-13278.

REFERENCES

Abt, H. A. 1983, ARA&A, 21, 343
Battaglia, G., et al. 2005, MNRAS, 364, 433
Baumgardt, H., Gualandris, A., & Portegies Zwart, S. 2006, MNRAS, 372, 174
Bellazzini, M., Ferraro, F. R., & Pancino, E. 2001, ApJ, 556, 635
Bonanos, A. Z., López-Morales, M., Hunter, I., & Ryans, R. S. I. 2008, ApJ, 675, L77
Bromley, B. C., & Kenyon, S. J. 2006, AJ, 131, 2737
Bromley, B. C., Kenyon, S. J., Geller, M. J., Barcikowski, E., Brown, W. R., & Kurtz, M. J. 2006, ApJ, 653, 1194
Brown, W. R., Beers, T. C., Wilhelm, R., Allende Prieto, C., Geller, M. J., Kenyon, S. J., & Kurtz, M. J. 2008, AJ, 135, 564
Brown, W. R., Geller, M. J., Kenyon, S. J., & Kurtz, M. J. 2005, ApJ, 622, L33
———. 2006a, ApJ, 640, L35
———. 2006b, ApJ, 647, 303
Brown, W. R., Geller, M. J., Kenyon, S. J., Kurtz, M. J., & Bromley, B. C. 2007a, ApJ, 660, 311
———. 2007b, ApJ, 666, 231
Bullock, J. S., & Johnston, K. V. 2005, ApJ, 635, 931
Dehnen, W., & Binney, J. 1998, MNRAS, 294, 429
Dehnen, W., McLaughlin, D. E., & Sachania, J. 2006, MNRAS, 369, 1688
Dib, S., Kim, J., & Shadmehri, M. 2007, MNRAS, 381, L40
Diemand, J., Kuhlen, M., & Madau, P. 2007, ApJ, 657, 262

Duquennoy, A., & Mayor, M. 1991, A&A, 248, 485
Eckart, A., & Genzel, R. 1997, MNRAS, 284, 576
Edelmann, H., Napiwotzki, R., Heber, U., Christlieb, N., & Reimers, D. 2005, ApJ, 634, L181
Eggleton, P. P. 1983, ApJ, 268, 368
Figer, D. F., Kim, S. S., Morris, M., Serabyn, E., Rich, R. M., & McLean, I. S. 1999, ApJ, 525, 750
Figer, D. F., et al. 2002, ApJ, 581, 258
Fuentes, C. I., Stanek, K. Z., Gaudi, B. S., McLeod, B. A., Bogdanov, S., Hartman, J. D., Hickox, R. C., & Holman, M. J. 2006, ApJ, 636, L37
Genzel, R., et al. 2003, ApJ, 594, 812
Ghez, A. M., Salim, S., Hornstein, S. D., Tanner, A., Lu, J. R., Morris, M., Becklin, E. E., & Duchêne, G. 2005, ApJ, 620, 744
Ginsburg, I., & Loeb, A. 2006, MNRAS, 368, 221
———. 2007, MNRAS, 376, 492
Gnedin, O. Y., Gould, A., Miralda-Escudé, J., & Zentner, A. R. 2005, ApJ, 634, 344
Gould, A., & Quillen, A. C. 2003, ApJ, 592, 935
Gualandris, A., Portegies Zwart, S., & Sipior, M. S. 2005, MNRAS, 363, 223
Hansen, B. M. S., & Milosavljević, M. 2003, ApJ, 593, L77
Heacox, W. D. 1998, AJ, 115, 325
Hernquist, L. 1990, ApJ, 356, 359
Hills, J. G. 1988, Nature, 331, 687
———. 1992, AJ, 103, 1955
Hirsch, H. A., Heber, U., O'Toole, S. J., & Bresolin, F. 2005, A&A, 444, L61
Hogg, D. W., Blanton, M. R., Roweis, S. T., & Johnston, K. V. 2005, ApJ, 629, 268
Kenyon, S. J., & Bromley, B. C. 2006, AJ, 131, 1837
Kenyon, S. J., & Hartmann, L. W. 1995, ApJS, 101, 117
Kim, S. S., Figer, D. F., Kudritzki, R. P., & Najarro, F. 2006, ApJ, 653, L113
Klypin, A., Zhao, H., & Somerville, R. S. 2002, ApJ, 573, 597
Kollmeier, J. A., & Gould, A. 2007, ApJ, 664, 343
Lada, C. J. 2006, ApJ, 640, L63
Lang, C. C., Johnson, K. E., Goss, W. M., & Rodríguez, L. F. 2005, AJ, 130, 2185
Launhardt, R., Zylka, R., & Mezger, P. G. 2002, A&A, 384, 112
Levin, Y. 2006, ApJ, 653, 1203
Lu, Y., Yu, Q., & Lin, D. N. C. 2007, ApJ, 666, L89
Merritt, D. 2006, Rep. Prog. Phys., 69, 2513
Miller, G. E., & Scalo, J. M. 1979, ApJS, 41, 513
Miyamoto, M., & Nagai, R. 1975, PASJ, 27, 533
Navarro, J. F., Frenk, C. S., & White, S. D. M. 1997, ApJ, 490, 493
O'Leary, R., & Loeb, A. 2008, MNRAS, 383, 86
Perets, H. B. 2007, ApJ, submitted (arXiv: 0712.1888)
Perets, H. B., Hopman, C., & Alexander, T. 2007, ApJ, 656, 709
Portegies Zwart, S., Gaburov, E., Chen, H.-C., & Gürkan, M. A. 2007, MNRAS, 378, L29
Rattenbury, N. J., Mao, S., Sumi, T., & Smith, M. C. 2007, MNRAS, 378, 1064
Salpeter, E. E. 1955, ApJ, 121, 161
Schaerer, D., Charbonnel, C., Meynet, G., Maeder, A., & Schaller, G. 1993, A&AS, 102, 339
Schaller, G., Schaerer, D., Meynet, G., & Maeder, A. 1992, A&AS, 96, 269
Schödel, R., Ott, T., Genzel, R., Eckart, A., Mouawad, N., & Alexander, T. 2003, ApJ, 596, 1015
Sesana, A., Haardt, F., & Madau, P. 2006, ApJ, 651, 392
———. 2007a, MNRAS, 379, L45
———. 2007b, ApJ, submitted (arXiv: 0710.4301)
Skrutskie, M. F., et al. 2006, AJ, 131, 1163
Stolte, A., Brandner, W., Grebel, E. K., Lenzen, R., & Lagrange, A.-M. 2005, ApJ, 628, L113
Stolte, A., Ghez, A. M., Morris, M. R., Lu, J. R., Brandner, W., & Matthews, K. 2008, ApJ, 675, 1278
Svensson, K. M., Church, R. P., & Davies, M. B. 2008, MNRAS, 383, L15
Tremaine, S., et al. 2002, ApJ, 574, 740
Widrow, L. M., & Dubinski, J. 2005, ApJ, 631, 838
Widrow, L. M., Pym, B., & Dubinski, J. 2008, ApJ, 679, 1239
Yi, S., Demarque, P., Kim, Y.-C., Lee, Y.-W., Ree, C. H., Lejeune, T., & Barnes, S. 2001, ApJS, 136, 417
Yoshida, H. 1990, Phys. Lett. A, 150, 262
Yu, Q., & Madau, P. 2007, MNRAS, 379, 1293
Yu, Q., & Tremaine, S. 2003, ApJ, 599, 1129